Cosmic Dynamics Unveiled: A Relativistic Approach to Structure Formation and Evolution in a Friedmann Universe

Kennedy Kamuren Konga , Dismas Simiyu Wamalwa * , Dickson Mwenda Kinyua , Patrick Njoroge Mwaniki , Daniel Maitethia

Posted Date: 10 September 2024

doi: 10.20944/preprints202409.0780.v1

Keywords: Redshift; Light intensity; Number density; Friedmann; Standard Model

Article

Cosmic Dynamics Unveiled: A Relativistic Approach to Structure Formation and Evolution in a Friedmann Universe

Kennedy Kamuren Konga [1], Dismas Simiyu Wamalwa [1,*], Dickson Kinyua Mwenda [2], Patrick Njoroge Mwaniki [1], Daniel Mumeu and Maitethia [1]

[1] Department of Physical Sciences, Meru University of Science and Technology, P.O Box 972-60200, MERU

[2] Department of Pure and Applied Sciences, Kirinyaga University, P.O.Box: 143-10300, KERUGOYA

* Correspondence: dismasw@yahoo.com.

Abstract: The advent of modern satellite technology has transformed observational astronomy and astrophysics, offering unprecedented insights into the large-scale behavior of gravitation and challenging established cosmological models. This technological progress has reinvigorated the study of relativistic cosmology, leading to a critical reassessment of foundational assumptions, particularly the cosmological principle, which posits that the universe is homogeneous and isotropic on large scales. While this principle underpins the Standard Cosmological Model and the Friedmann-Lemaitre-Robertson-Walker metric, emerging data has increasingly been challenging its validity. Central to this investigation are the redshift-distance and light intensity-distance relations, essential for testing cosmological models. The integration of both parametric and nonparametric redshift models provides a more comprehensive analysis, addressing discrepancies in our understanding of the universe's structure and evolution. However, unresolved mysteries, particularly concerning dark matter and dark energy, complicate these models. This research critically examines the cosmological principle using the latest observational data and scrutinizes the Friedmann model's assumptions. The study shows that galaxy formation was most rapid in the early universe, especially within the redshift range of $0 < z < 0.8$, with notable peaks around at $z \approx 0.1$ and $z \approx 0.5$. These two characteristic redshift values, predicted by our standard Friedmann redshift model used in this work, are confirmed by the observational data utilized in this research. The research also highlights that dark matter plays a significantly more critical role than dark energy in the process of galaxy formation. While dark energy primarily affects the large-scale expansion of the universe, dark matter seems to go beyond the domination of local galaxy formation and evolution of cosmic structures. These findings underscore the limitations of current models and contribute to the ongoing refinement of cosmological theories, offering a clearer understanding of the universe's evolution.

Keywords: Redshift-light intensity- structure formation-number density-standard cosmological model-Friedmann

1. Introduction

The homogeneity of matter distribution at large scales, known as the cosmological principle (CP), is a central assumption in the standard cosmological model (SCM). Rooted in a geometrical assumption outlined by Einstein in 1917, the cosmological principle posits that on a vast scale, the spatial distribution of matter is both homogeneous and isotropic [1]. Despite the apparent lack of homogeneity and isotropy at small scales in the distributions of celestial objects, the cosmological principle implies the existence of a homogeneity scale, beyond which the distribution becomes

 doi:10.20944/preprints202409.0780.v1

statistically indistinguishable from a random one bringing the argument of whether or not the universe is homogeneous or fractal in nature as the scale evolves with time [2].

In contemporary cosmological models within the framework of general relativity, the Friedmann-Lemaitre-Robertson-Walker (FLRW) metric serves as the common basis [3]. Distinctions among these models arise not from the solutions to Einstein's equations but from the selection of the stress-energy tensor ($T_{\mu\nu}$), specifically influencing the expansion factor, R(t), in the spatial line element [4].

The SCM builds upon two fundamental tenets: the consideration of General Relativity as the foundational theory of gravity and the adherence to the CP, positing statistical homogeneity and isotropy at large scales [5]. The CP, in its modern formulation, dictates that, at sufficiently large scales, the average evolution of the universe precisely adheres to the FLRW metric [6]. While the homogeneous SCM model aligns well with observations, challenges such as the fine-tuning problems, Hubble tension, and cosmic coincidence issues suggest potential deviations from the SCM [7–9]. Key to this discussion are the redshift-distance and light intensity-distance relations, which are fundamental tools in observational cosmology. The redshift-distance relation provides critical insights into the universe's expansion rate, serving as a direct test of cosmological models. Accurate measurements of redshift and corresponding distances allow cosmologists to map the large-scale structure of the universe, revealing patterns that either support or challenge the assumptions of homogeneity and isotropy. Similarly, the light intensity-distance relation, which describes how the observed brightness of an object diminishes with distance, is crucial for determining cosmological distances and, by extension, for understanding the universe's expansion history. Both relations are integral to testing the validity of the Friedmann model and the cosmological principle, particularly in light of the growing complexity observed in deep-space surveys.

To refine our understanding of these relations, recent studies have employed both parametric and nonparametric redshift models. Parametric models rely on predefined functional forms and assumptions about the universe’s expansion history, such as the commonly used SCM model, which assumes a specific functional form for the expansion rate and matter density[10]. Nonparametric models, on the other hand, do not assume a particular functional form and instead use data-driven approaches to infer the redshift-distance relation directly from observations [11]. These models offer greater flexibility and can capture deviations from the standard parametric assumptions, providing a more nuanced view of the universe's structure and evolution [5,12]. The integration of both parametric and nonparametric approaches allows for a more comprehensive analysis of the redshift-distance relation, potentially addressing discrepancies and refining our understanding of cosmological principle.

Compounding these theoretical challenges are the enigmatic dark matter (DM) and dark energy (DE), which together make up 95% of the universe's total mass-energy content. While DM is crucial for explaining the flat rotation curves of galaxies and the formation of large-scale structures, DE has been claimed to account for the observed acceleration in the universe's expansion—a phenomenon first detected through observations of Supernovae Type Ia [13]. Nevertheless, the physical nature of these two phenomena remains a mystery. Einstein suggested a long-forgotten solution: gravitationally repulsive negative masses, which drive cosmic expansion and cannot coalesce into light-emitting structures [14]. In addition, a type of cold dark matter in the universe is needed to explain the formation of the cosmic structure and galaxy dynamics. So far, it has been claimed that the cosmological constant is the best candidate to explain the so-called dark energy [5]. These unresolved issues further complicate the cosmological models, demanding more precise observational data and innovative theoretical approaches.

The challenge of testing the cosmological principle and the SCM is further exacerbated by the limitations of current observational methods. Three-dimensional redshift surveys, despite their sophistication, often produce limited and potentially misleading data due to inherent uncertainties in cosmic distance measurements and the complexity of interpreting large-scale structures. For instance, while observational evidence generally supports isotropy on large scales—demonstrated by the Cosmic Microwave Background Radiation (CMBR), and isotropic distributions of radio sources,

 doi:10.20944/preprints202409.0780.v1

gamma-ray bursts, and supernovae [15,16] findings do not unequivocally confirm large-scale homogeneity. In particular, quasar distribution studies suggest homogeneity only beyond scales of $250\ h^{-1}$ Mpc [17], , highlighting the need for more rigorous testing.

In light of the unsettling discoveries detailed above, there exists a pervasive sense of uncertainty regarding the accuracy of current cosmological frameworks. To this regard, we present a model describing the universe's dynamics, structure formation and evolution by taking into account its density and geometry. The investigation centers on three astronomical parameters: number density, light intensity, and redshift. We analyze the evolution of number density and light intensity across redshift, assessing their influence from the universe's infancy to the present, and conduct a comparative evaluation with findings from other studies. In particular, we shall make comparisons with works of Langa et al. (2017) whose model we shall refer to as 'approximate standard Friedmann redshift model' and Nyagisera et al. (2024) whose model we shall refer to as 'modified standard Friedmann redshift model'. The model developed in this paper shall be referred to as the 'standard Friedmann redshift model'. Throughout our examination, we shall account for the influence exerted by dark matter and dark energy within these theoretical constructs. In order to validate our model, a histogram plot of observational data of galactic number count against redshift extracted from NASA/IPAC Extragalactic Database shall be performed.

The paper is structured as follows: Section 2 introduces our model, Sections 3 and 4 presents the analytical and graphical results of our study respectively, while Sections 5 is devoted to discussions of our results before culminating into conclusions in Section 6.

2. Model Formulation

2.1. Parametric Model

The parametric model introduced by Bassett et al. [10] in 2015 modifies the conventional redshift framework to enhance our understanding of cosmic dynamics. By introducing parameters that adjust the redshift space, this model allows for a more refined interpretation of observational data. It also tackles intricate aspects of cosmic phenomena by incorporating these specific parameters, offering a more precise and detailed representation of redshift-related observations. In this study, we shall compare our model with the parametric model $f(z) = \alpha_1 z + \alpha_2 z^2$ where c1 and c2 are arbitrary parameters (see details in Nyagisera et al., 2024).

2.2. Nonparametric Model

The non-parametric model developed by Wojtak and Prada [11] in 2017 adopts a different approach by avoiding predefined parameters, offering greater flexibility in modeling cosmic phenomena. Unlike parametric models, this non-parametric model does not impose fixed parameters, allowing for a more adaptive and data-driven analysis of redshift-related phenomena. In this work, we shall compare our model with the nonparametric model
$f(z) = z + \gamma(z)^2$ where $\gamma(z)$ is a freely varying function of z (see details in Nyagisera et al., 2024).

2.3. The Einstein Field Equations Based on Friedmann Model

Consider the FLRW metric

$$ds^2 = c^2dt^2 - \frac{R(t)}{(1+\kappa r^2)^2}dr^2 \tag{1}$$

where c is the speed of light, $R(t)$, denotes the scale factor governing the time-dependent evolution of the spatial portion of the metric (specifically, the surfaces corresponding to constant time, t), $\kappa = (-1,0,1)$ gives the geometry of the universe as open, flat, or closed respectively, and $dr^2 = dx^2 + dy^2 + dz^2$ is the rectangular coordinate representation of the three dimensional projection space.

Straightforward calculations based on equation (1) [12,19,20] yield:

 doi:10.20944/preprints202409.0780.v1

$$12\kappa c^2 + 3R'(t)^2 = \beta c^4 \rho(t) R(t)^2 - \lambda c^2 R(t)^2 \quad (2)$$

$$4\kappa c^2 + 2R(t)R''(t) + R'(t)^2 = \beta c^2 \rho(t) R(t)^2 - \lambda c^2 R(t)^2 \quad (3)$$

where $R(t)' = \frac{dR}{dt}$, $R(t)'' = \frac{d^2R}{dt^2}$, $\rho(t)$ is the density of the observable universe and $\beta = \frac{8\pi G}{c^4}$

Equations (2) and (3) are key in describing the dynamics, formation of structures and evolution of the universe. Earlier studies [12,20] used the Noether theorem pertinent to a matter-dominated Friedmann universe;

$$\rho(t)R(t)^3 = \alpha$$

This theorem deduced Einstein field equations relation of the form

$$\mathrm{dt} = \frac{\mathrm{dR(t)}}{\sqrt{\frac{(\beta c^4 \rho(t) - \lambda c^2)\alpha}{3\rho(t)R(t)} - 4\kappa c^2}} \quad (4)$$

In contrast to these studies, this work treated the density of the universe and the cosmic scale factor as variables thus rearranged equation (2) to yield;

$$dt = \frac{dR(t)}{\sqrt{\frac{(\beta c^4 \rho(t) - \lambda c^2)R(t)^2}{3} - 4\kappa c^2}} \quad (5)$$

Equation (4) and equation (5) is the Friedmann model relation representing time taken by a light photon to travel a distance dr, describing the Friedmann Universe. Equation (5) brings a clearer description of the dynamics, structure formation and evolution of the universe as compared to equation (4) obtained through conservation theorem in existing works [12,20]. Equation (5) will be applied in deriving the light intensity-redshift and the number density-redshift relations in this work.

3. Analytical solutions

3.1. Light Intensity-Redshift Relation

Considering light emanating from an astronomical object (galaxy or a star) commencing its journey at $r(t_e)$ and progressing towards the spatial origin, $r = r(t_o)$, when time $t = t_o$. In this scenario, the FLRW metric (see Equation (1)) can be formulated to capture this dynamic spatial relationship for null geodesic as;

$$0 = c^2 \dot{t}^2 - \frac{R(t)^2}{(1 + \kappa r^2)^2} \dot{r}^2 \quad (6)$$

where $\frac{dt}{d\tau} = \dot{t}, \frac{dr}{d\tau} = \dot{r}$ implying that

$$c\dot{t} = \pm \frac{R(t)}{1 + \kappa r^2} \dot{r} \quad (7)$$

Performing integration of equation (7) over (t_e, to) and $(r(t_e), r(t_o))$ and applying the reversibility of light principle while noting that $\dot{t}$ positive while $\dot{r}$ negative by our assumption,

$$\int_{t_e}^{t_o} \frac{c}{R(t)} dt = -\int_{r(t_e)}^{r(t_o)} \frac{1}{1 + \kappa r^2} dr \quad (8)$$

Substituting equation (5) into equation (8) gives :

$$\int_{R(t_e)}^{R(t_o)} \frac{dR(t)}{R(t)^2 \sqrt{\frac{(\beta c^2 \rho(t) - \lambda)}{3} - \frac{4\kappa}{R(t)^2}}} = -\int_{r(t_e)}^{r(t_o)} \frac{dr}{1 + \kappa r^2} \quad (9)$$

Preprints.org (www.preprints.org) | NOT PEER-REVIEWED | Posted: 10 September 2024 doi:10.20944/preprints202409.0780.v1

Equation (9) is more general and is suitable for describing the evolution and dynamics of the universe as it contains an extra cosmological term on its L.H.S earlier present in equation (5). Solving this equation for three different cases of κ, that is, for open universe ($\kappa = -1$), flat universe($\kappa = 0$), and for a closed universe($\kappa = 1$), it can easily be shown that:

$$r(t_e) = \begin{cases} \dfrac{z}{aR(t_o)} & for\ k = 0, \\ \dfrac{2(1+z)\left(aR(t_o) + \sqrt{(aR(t_o))^2 - 4}\right) - 2\left(aR(t_o) + \sqrt{(aR(t_o))^2 - 4(1+z)^2}\right)}{\left(aR(t_o) + \sqrt{(aR(t_o))^2 - 4(1+z)^2}\right)\left(aR(t_o) + \sqrt{(aR(t_o))^2 - 4}\right) + 4(1+z)} & for\ k = -1, \\ \dfrac{2\left[(1+z)\left(aR(t_o) + \sqrt{a^2R(t_o)^2 + 4}\right) - \left(aR(t_o) + \sqrt{a^2R(t_o)^2 + 4(1+z)^2}\right)\right]}{\left(aR(t_o) + \sqrt{a^2R(t_o)^2 + 4}\right)\left(aR(t_o) + \sqrt{a^2R(t_o)^2 + 4(1+z)^2}\right) - 4(1+z)} & for\ k = 1 \end{cases} \quad (10)$$

where

$$a = \sqrt{\frac{(\beta c^2 \rho(t) - \lambda)}{3}}$$

The three cases in equation (10) can be generalized as

$$r(z) = \frac{2\left[(1+z)\left(aR(t_o) + \sqrt{a^2R(t_o)^2 - 4\kappa}\right) - \left(aR(t_o) + \sqrt{a^2R(t_o)^2 - 4\kappa(1+z)^2}\right)\right]}{\left(aR(t_o) + \sqrt{a^2R(t_o)^2 - 4\kappa}\right)\left(aR(t_o) + \sqrt{a^2R(t_o)^2 - 4\kappa(1+z)^2}\right) + 4\kappa(1+z)} \quad (11)$$

where $\kappa = -1,0,1$, $r(t_e) = r(z)$ since t_e depends on z, $R(t_e) = R(t_o)/(1+z)$ and $\rho(t)$ is the density of the universe at observational time, t_o.

Equation (11) can be decomposed to;

$$r(z) = \frac{2(p(1+z) - q)}{pq + 4\kappa(1+z)} \quad (12)$$

where,

$$p = aR(t_o) + \sqrt{a^2R(t_o)^2 - 4\kappa}$$

and

$$q = aR(t_o) + \sqrt{a^2R(t_o)^2 - 4\kappa(1+z)^2}$$

Consider an astronomical object, whether it be a luminous star or a galaxy, positioned at the origin, $r(t_o) = 0$, emitting light with absolute luminosity, L. Over a time, span of emission, t_e, we contemplate the emission of light, each increment of which is encapsulated by dt_e. Subsequently, at a distinct moment of observation, t_o, an observer gauges the intensity of the emitted light, I, which is inevitably subject to a redshift z. The spatial coordinates of the observer are elegantly captured by Equation (11). This intricate interplay of emission, transmission, and observation culminates in Equation (13), expressed as:

$$I = \frac{L dt_e}{(1+z) S_{r(z)}} \quad (13)$$

where $S_{r(z)} = \frac{4\pi r(z)^2 R(t_o)^2}{(1+\kappa r^2)^2}$ is the surface area of the sphere of radius $r = r(z)$ at time $t = t_o$ [20].

Applying equation (12) in equation (13) and the fundamental theorem of integral calculus together with the relation $\frac{dt_e}{dt_o} = \frac{R(t_e)}{R(t_o)} = \frac{1}{1+z}$, we obtain:

$$I = \frac{L\left[1 + \kappa\left(\frac{2(p(1+z) - q)}{pq + 4\kappa(1+z)}\right)^2\right]^2}{4\pi\left(\frac{2(p(1+z) - q)}{pq + 4\kappa(1+z)}\right)^2 R^2(t_o)(1+z)^2} \quad (14)$$

 doi:10.20944/preprints202409.0780.v1

Equation (14) unveils a profound connection between redshift z and the luminous intensity I. This equation serves as a pivotal conduit, allowing us to delve into the dynamics and evolution of the our universe.

3.2. Number Density Redshift Relation

Let us direct our focus toward celestial bodies, galaxies or supernovae for instance, which exhibit uniform distribution across the expanse of the universe within specific range of redshift. In this context, let N symbolize the number of galaxies existing per unit volume within a spatial metric denoted as $(dr^2 + r^2d\theta^2 + r^2sin^2\theta d\theta)/(1+\kappa r^2)^2$. Additionally, the volume element $r^2sin\theta d\theta d\varphi dr/(1+\kappa r^2)^3$ encapsulates the spatial dimensions. This framework enables us to delineate the population of galaxies spanning the range from r to dr , expressed as $4\pi r^2dr/(1+\kappa r^2)^3$ [19]. Subsequently, the number of galaxies between coordinate hyperspheres $r(z)$ and $r(z+dz)$ is given by

$$n(z)dz = \frac{4\pi r(z)^2 N r'(z)dz}{(1+kr(z)^2)^3} \tag{15}$$

Differentiating Equation (11) with respect to z and using equation (12) yield;

$$\mathrm{r'(z)} = \frac{2(\mathrm{x}(\mathrm{x}-\mathrm{aR(t_o)}) - \mathrm{y}(\mathrm{y}-\mathrm{aR(t_o)})}{(\mathrm{q}-\mathrm{aR(t_o)x^2}} \tag{16}$$

where $r'(z) = dr/dz$, $\mathrm{x} = \mathrm{pq} + 4\kappa(1+\mathrm{z})$ and $\mathrm{y} = \mathrm{p}(1+\mathrm{z}) - \mathrm{q}$

Substituting Equation (12) and Equation (16) into Equation (15) gives;

$$\mathrm{n(z)} = \frac{32\pi(\mathrm{p}(1+\mathrm{z})-\mathrm{q})^2\mathrm{N}\left(\mathrm{x}(\mathrm{x}-\mathrm{aR(t_o)}) - \mathrm{y}(\mathrm{y}-\mathrm{aR(t_o)})\right)}{\left(\mathrm{pq}+4\mathrm{k}(1+\mathrm{z})\right)^2((\mathrm{q}-\mathrm{aR(t_o)x^2})\left(1+\kappa\left(\frac{2(\mathrm{p}(1+\mathrm{z})-\mathrm{q})}{\mathrm{pq}+4\kappa(1+\mathrm{z})}\right)^2\right)^3} \tag{17}$$

Equation (17) relates the evolution of the number density of astronomical objects with redshift in the Friedmann universe, which together with equation (14) constitutes the fundamental results in this paper.

4. Graphical Results

In the preceding section, we derived the interplay between galactic number density, redshift, and light intensity through analytical methods. We shall now transition to a visual exploration of our established outcomes, achieved through the development and execution of straightforward MATLAB programs. By implementing these programs, we are poised to generate graphical representations that illustrate the relationships between light intensity and redshift, as well as between number density and redshift, as dictated by equations (14) and (17) respectively. The range of redshift values employed in our MATLAB simulations spans from $z = 0$ to $z = 5$, a spectrum that aligns harmoniously with existing statistical data and observations. This methodology permits us to illuminate the empirical significance of our theoretical constructs and enhance our grasp of the cosmic evolution landscape.

The program encompasses a range of universe densities, spanning from $\rho(t) = 3\times10^{-27}\,kg/m^3$ to $\rho(t) = 6.23\times10^{-23}\,kg/m^3$. The velocity of light $c = 3\times10^8\,m/s$, the cosmic scale factor, $R(t_o) = 9\times10^{25}\,m$, while the gravitational constant $G = 6.67\times10^{-11}\,m^3/kg/s^2$. The universe's curvature, κ assumes values of $-1, 0,$ and 1, and the cosmological constant $\lambda = 1.19\times10^{-52}\,m^{-2}$. To enhance accuracy, logarithms of light intensity and number density are employed. For our exploration, we assign arbitrary values of 1 to the parameters N (number of galaxies per unit volume) and L (absolute power of a galaxy or star). This approach facilitates the determination of parameter combinations ρ and $R(t_o)$ that best align with experimental data without presuming assumptions about background geometry.

4.1. Light Intensity Redshift Relation

 doi:10.20944/preprints202409.0780.v1

Executing our program using equation (14) for different $\rho(t)(kg/m^3)$ and κ values yield the ensuing outcomes (refer to Figures 1 to 14) pertinent to light intensity.

Figures 1-14 show the relationship between light intensity and redshift. The Y-axis (Log I) shows the logarithm of light intensity, where lower values correspond to reduced intensity. The X-axis (Redshift, z) tracks the evolution of the universe from its inception at $z = 0$. Different initial values of log(I) across the curves indicate varying light intensities based on the universe's density (ρ) and curvature (κ).

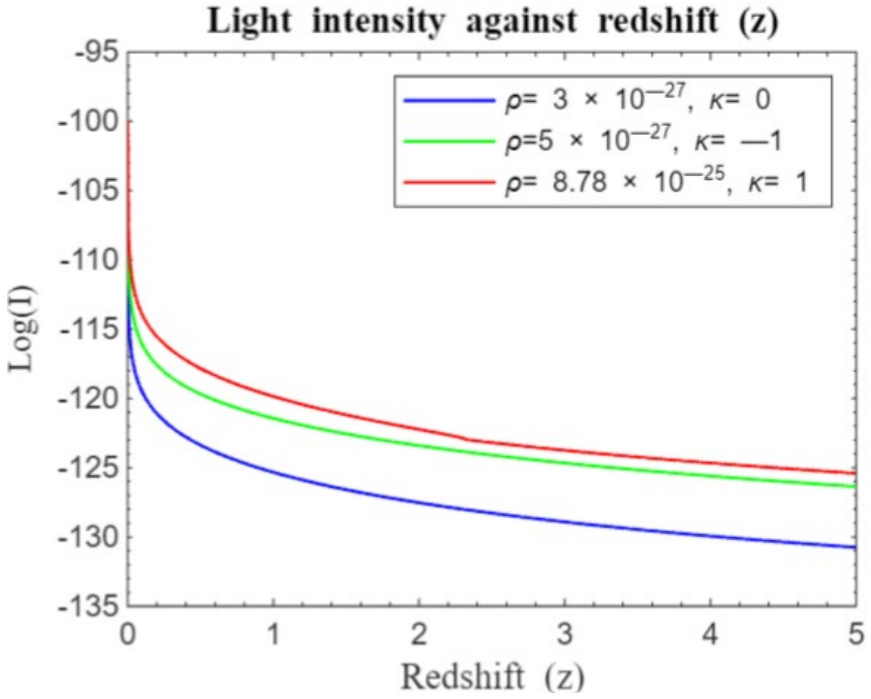

Figure 1. Simulation result for log (n) against redshift z for $\mathbf{z = 0}$ to $\mathbf{z = 5}$ of the standard Friedmann redshift model without $\boldsymbol{\lambda}$.

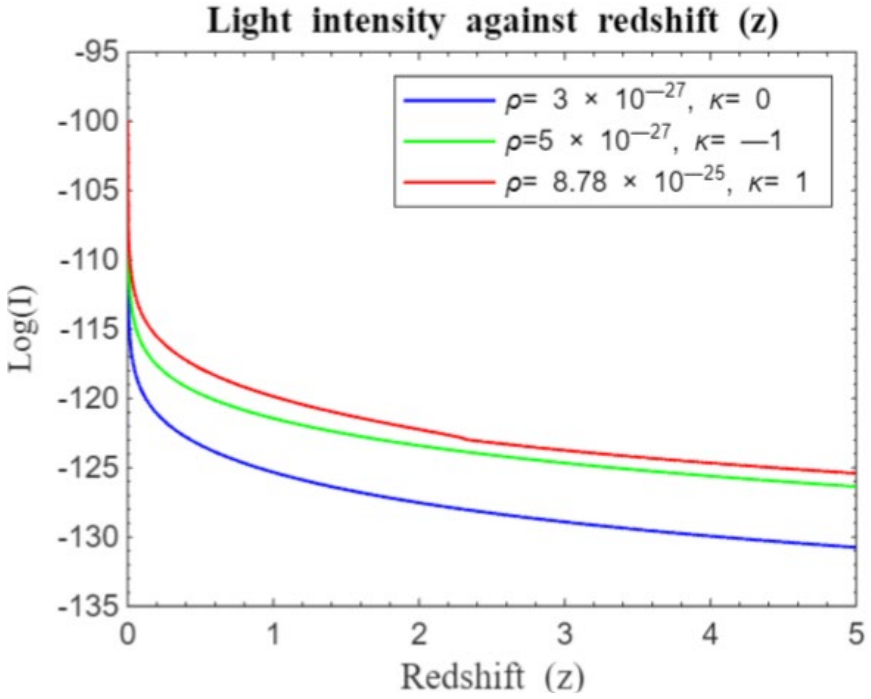

Figure 2. Simulation result for log (n) against redshift z for $\mathbf{z = 0}$ to $\mathbf{z = 5}$ of the standard Friedmann redshift model with $\boldsymbol{\lambda}$.

 doi:10.20944/preprints202409.0780.v1

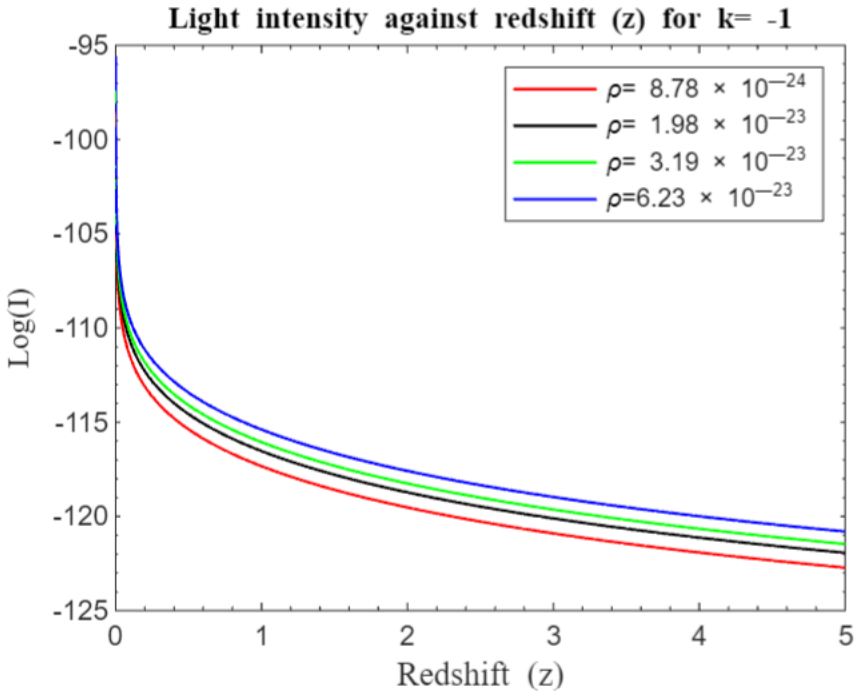

Figure 3. Simulation result for log (n) against redshift z for $\mathbf{z = 0}$ to $\mathbf{z = 5}$ of the standard Friedmann redshift model for an open universe without $\boldsymbol{\lambda}$.

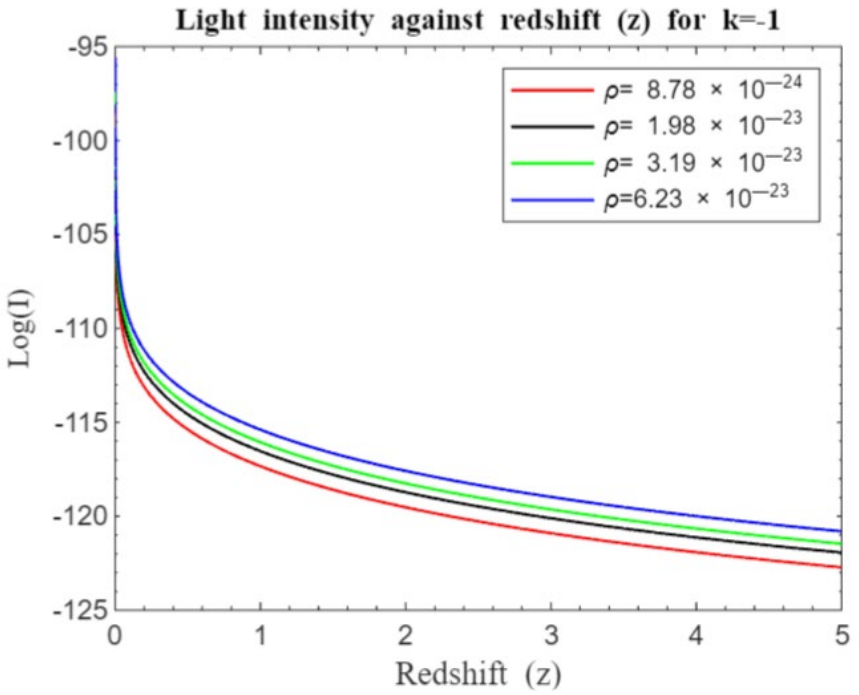

Figure 4. Simulation result for log (n) against redshift z for $\mathbf{z = 0}$ to $\mathbf{z = 5}$ of the standard Friedmann redshift model for an open universe with $\boldsymbol{\lambda}$.

Preprints.org (www.preprints.org) | NOT PEER-REVIEWED | Posted: 10 September 2024 doi:10.20944/preprints202409.0780.v1

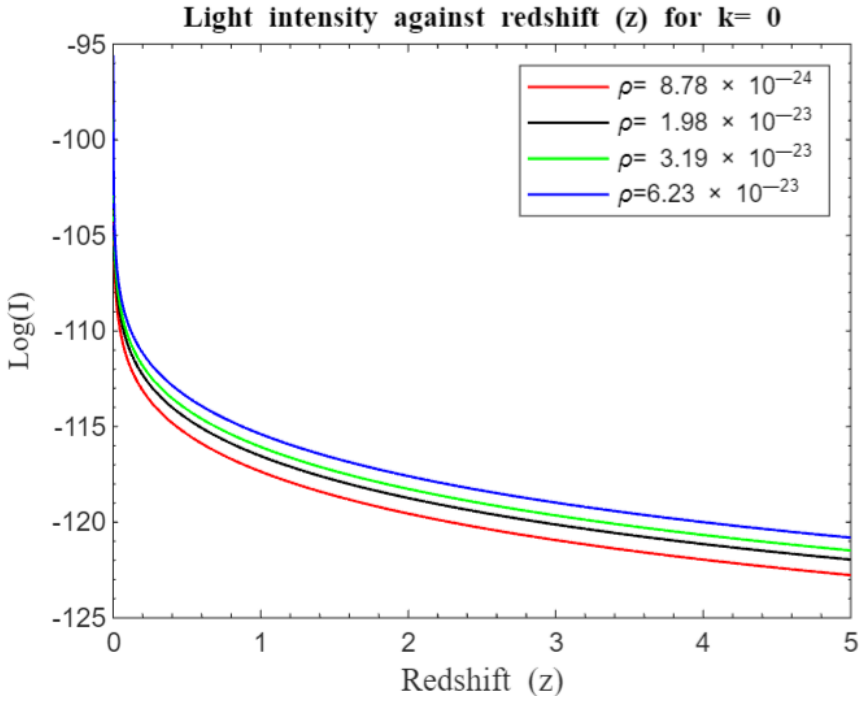

Figure 5. Simulation result for log (n) against redshift z for $\mathbf{z = 0}$ to $\mathbf{z = 5}$ of the standard Friedmann redshift model for a flat universe without **λ**.

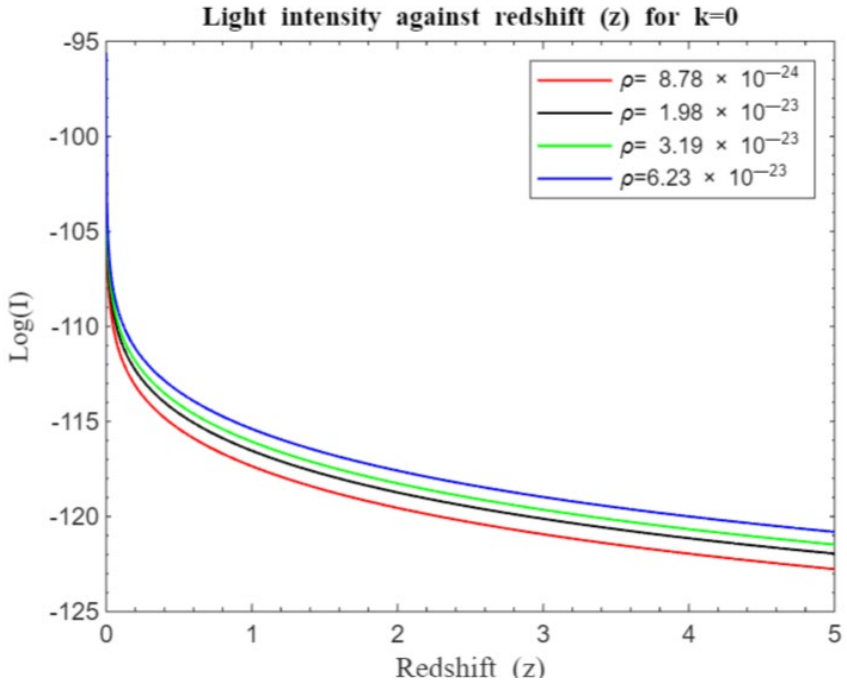

Figure 6. Simulation result for log (n) against redshift z for z=0 to z=5 of the standard Friedmann redshift model for a flat universe with λ.

Preprints.org (www.preprints.org) | NOT PEER-REVIEWED | Posted: 10 September 2024 doi:10.20944/preprints202409.0780.v1

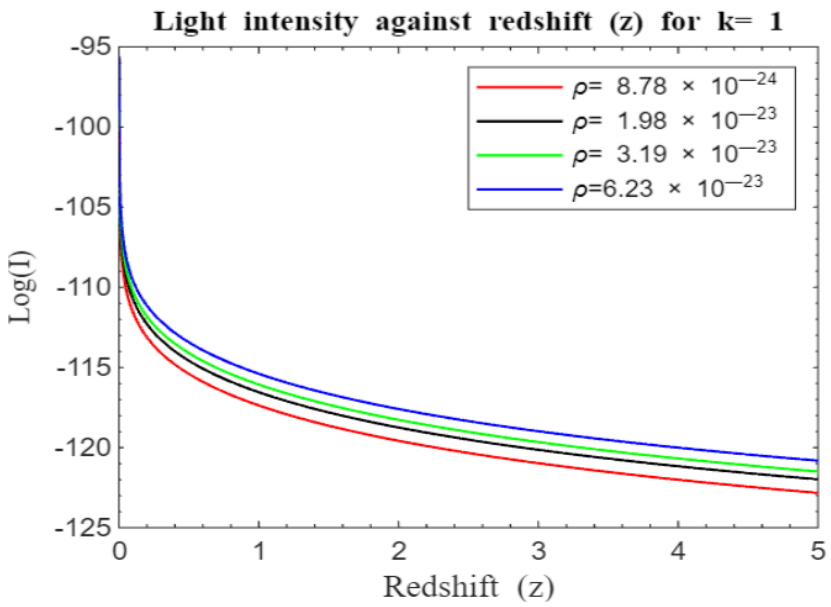

Figure 7. Simulation result for log (n) against redshift z for z=0 to z=5 of the Standard Friedmann redshift model for a closed universe without λ.

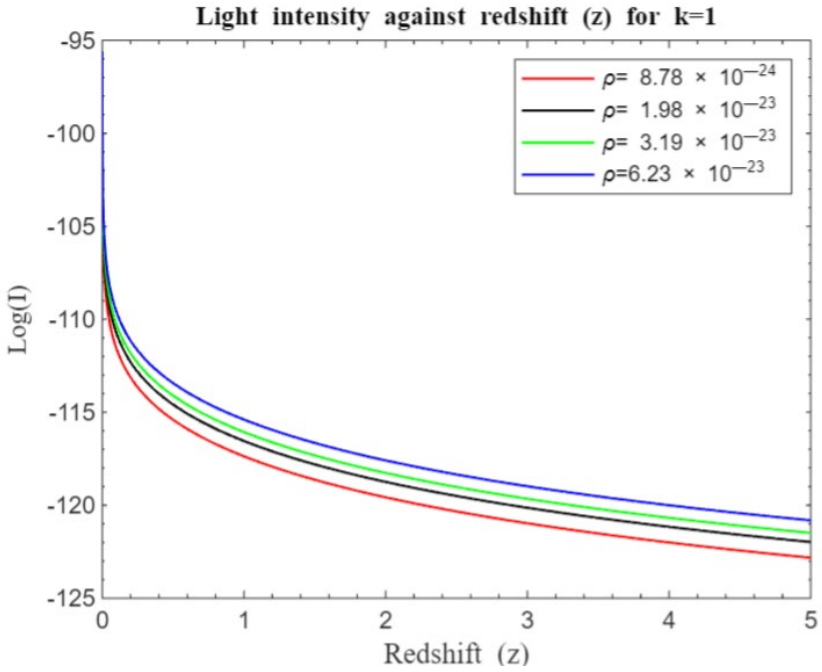

Figure 8. Simulation result for log (n) against redshift z for z=0 to z=5 of the standard Friedmann redshift model for a closed universe with λ.

Preprints.org (www.preprints.org) | NOT PEER-REVIEWED | Posted: 10 September 2024 doi:10.20944/preprints202409.0780.v1

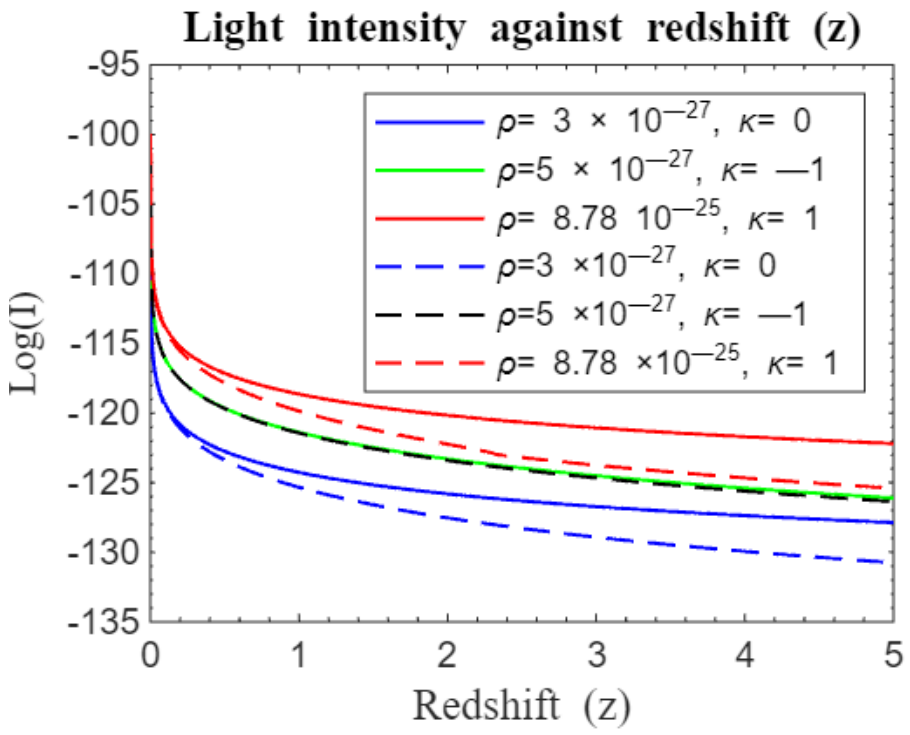

Figure 9. Simulation result for log (I) against redshift z for **z = 0** to **z = 5**. The solid curves represent the approximate standard Friedmann redshift model while dotted curves represent the standard Friedmann redshift model. Both models without λ.

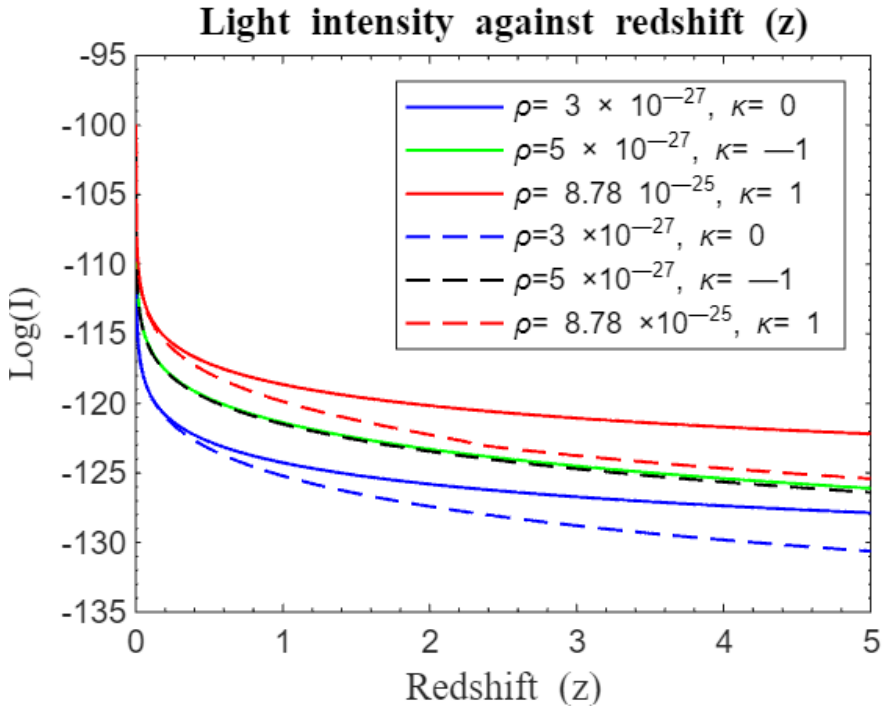

Figure 10. Simulation result for log (I) against redshift z for **z = 0** to **z = 5**. The solid curves represent the approximate standard Friedmann redshift model without **λ** while dotted curves represent the standard Friedmann redshift model with **λ**.

Preprints.org (www.preprints.org) | NOT PEER-REVIEWED | Posted: 10 September 2024 doi:10.20944/preprints202409.0780.v1

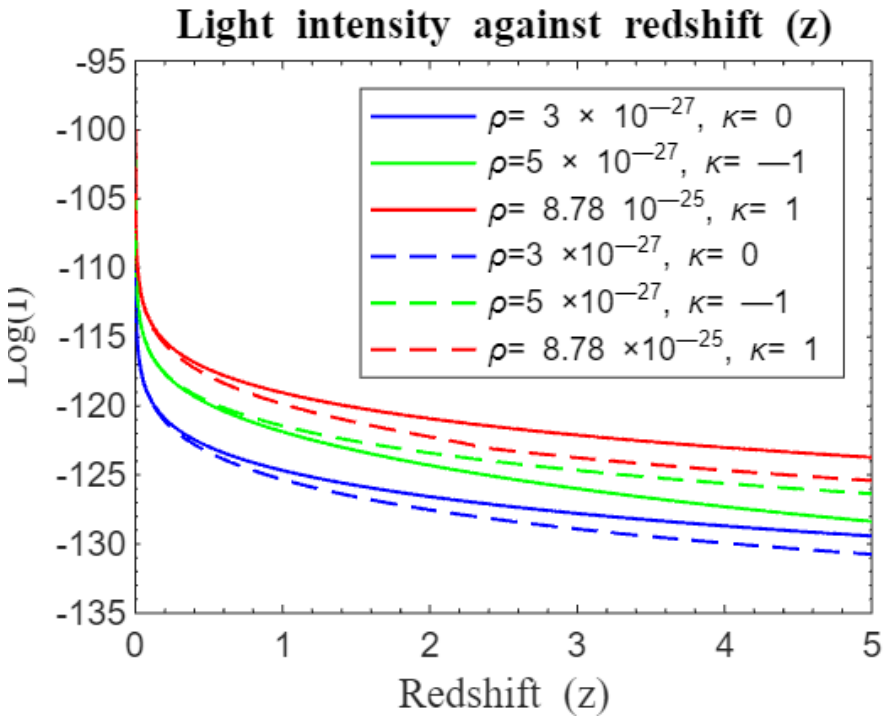

Figure 11. Simulation result for log (I) against redshift z for $\mathbf{z = 0}$ to $\mathbf{z = 5}$. The solid curves represent the modified standard Friedmann redshift model $\mathbf{f(z) = z + \gamma(z)^2}$ with $\boldsymbol{\gamma = 0.45}$ while the dotted curves represent the Standard Friedmann Redshift Model. Both models without λ.

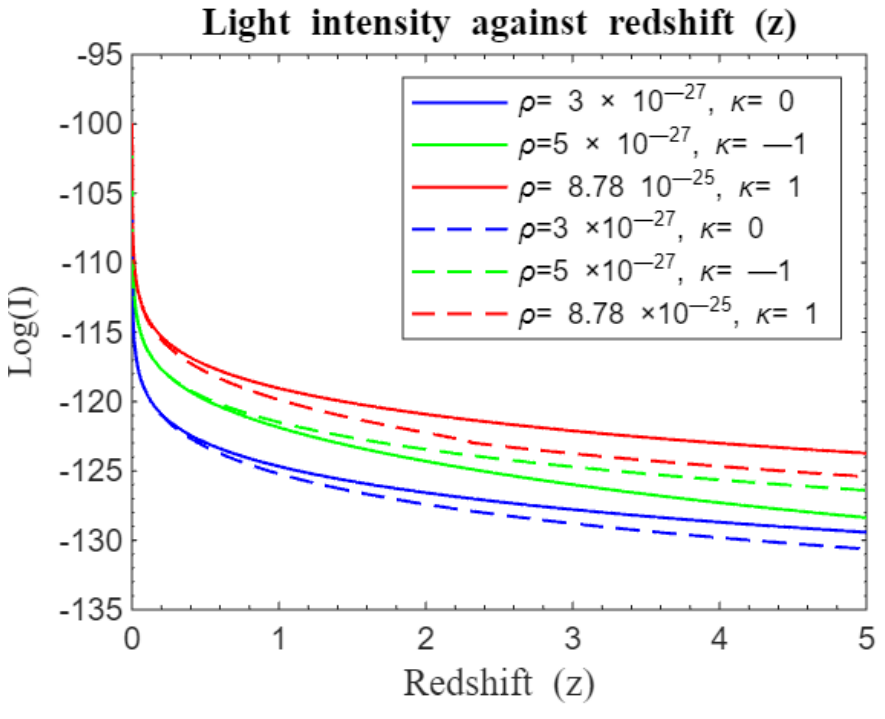

Figure 12. Simulation result for log (I) against redshift z for $\mathbf{z = 0}$ to $\mathbf{z = 5}$. The solid curves represent the modified standard Friedmann redshift model $\mathbf{f(z) = z + \gamma(z)^2}$ with $\boldsymbol{\gamma = 0.45}$ without $\boldsymbol{\lambda}$ while dotted curves represent the standard Friedmann redshift model with $\boldsymbol{\lambda}$.

Preprints.org (www.preprints.org) | NOT PEER-REVIEWED | Posted: 10 September 2024 doi:10.20944/preprints202409.0780.v1

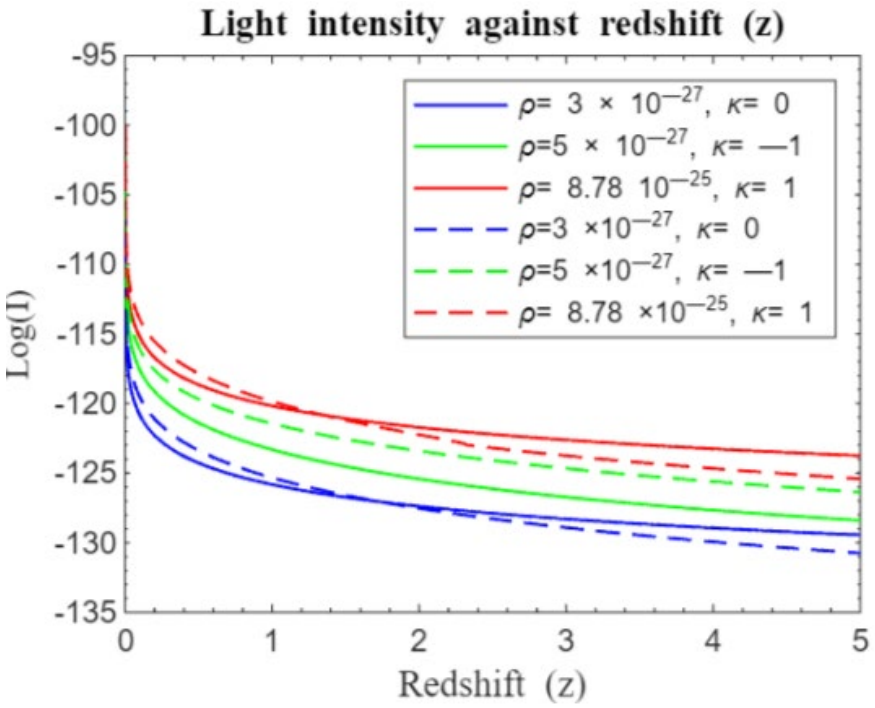

Figure 13. Simulation result for log (I) against redshift z for $\mathbf{z = 0}$ to $\mathbf{z = 5}$. The solid curves represent the modified standard Friedmann redshift model $\mathbf{f(z) = \alpha_1 z + \alpha_2 z^2}$ with $\boldsymbol{\alpha_1 = 2.005}$ and $\boldsymbol{\alpha_2 = 0.005}$ while dotted curves represent the standard Friedmann redshift model. Both models without λ.

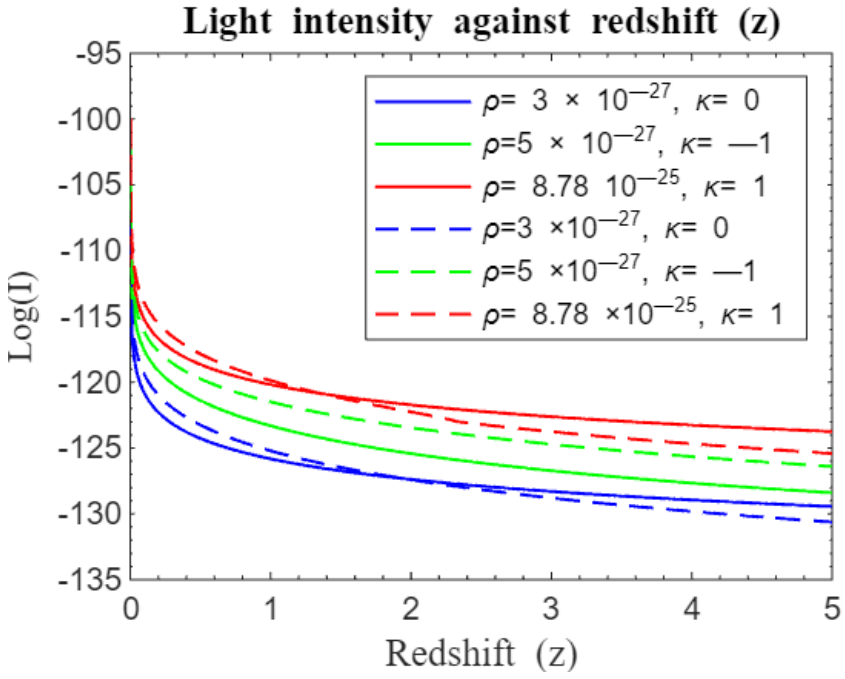

Figure 14. Simulation result for log (I) against redshift z for $\mathbf{z = 0}$ to $\mathbf{z = 5}$. The solid curves represent the modified standard Friedmann redshift model $\mathbf{f(z) = \alpha_1 z + \alpha_2 z^2}$ with $\boldsymbol{\alpha_1 = 2.005}$ and $\boldsymbol{\alpha_2 = 0.005}$ without $\boldsymbol{\lambda}$ while dotted curves represent the standard Friedmann redshift models with $\boldsymbol{\lambda}$.

4.2. Number Density Redshift Relation

Figures 15-28 show the evolution of galaxy number density, $n(z)$, in relation to redshift z, as described by equation (17). The Y-axis (Log n) shows the logarithm of number density, where lower

Preprints.org (www.preprints.org) | NOT PEER-REVIEWED | Posted: 10 September 2024 doi:10.20944/preprints202409.0780.v1

values correspond to reduced density. The X-axis (Redshift, z) tracks the evolution of the universe from its inception at $z = 0$. Different initial values of Log(n) across the curves indicate varying number densities based on the density (ρ) of the universe and its curvature, κ.

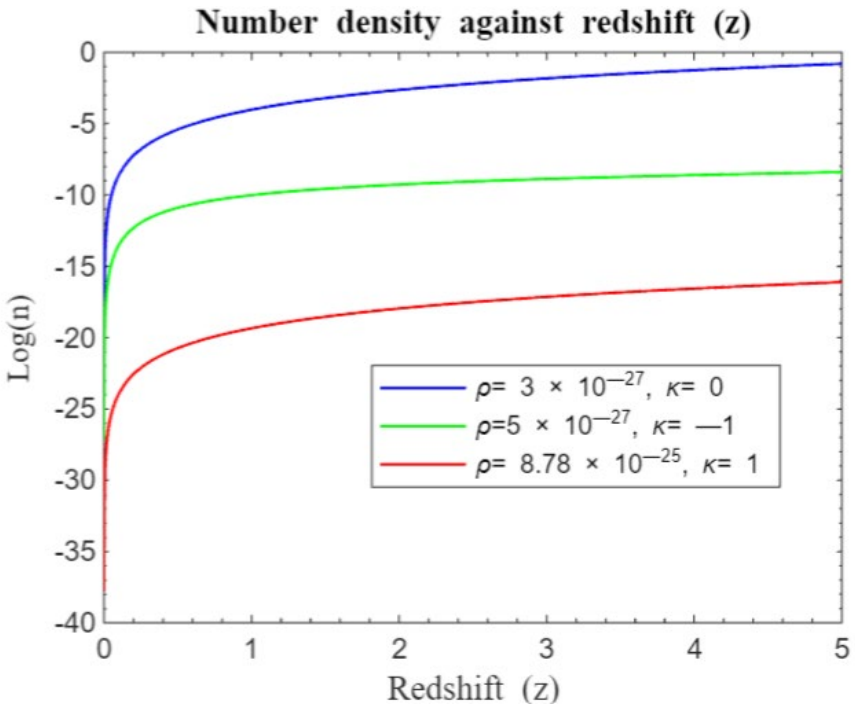

Figure 15. Simulation result for log (n) against redshift z for $\mathbf{z = 0}$ to $\mathbf{z = 5}$ of the standard Friedmann redshift model without $\boldsymbol{\lambda}$.

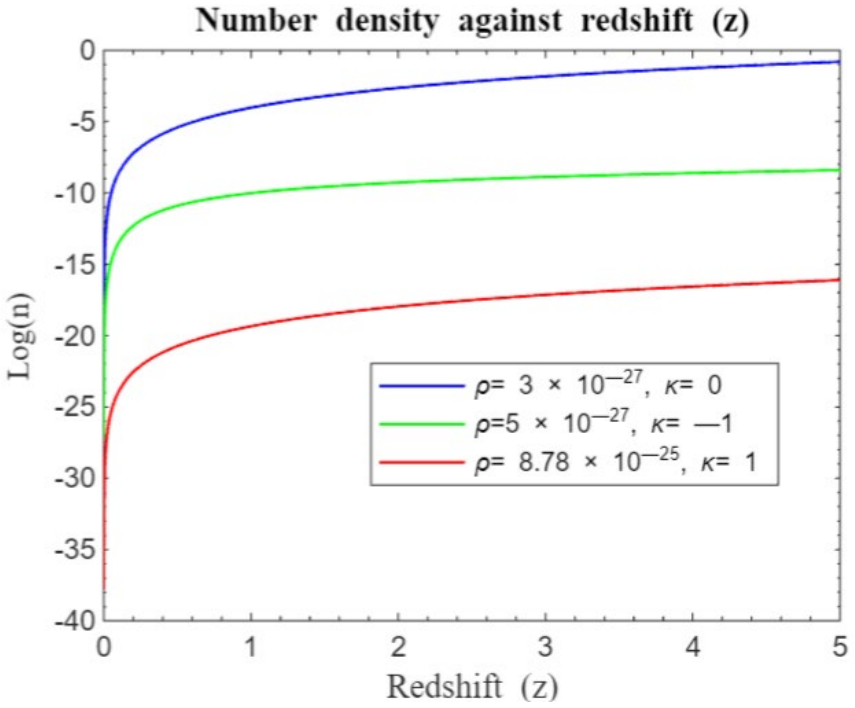

Figure 16. Simulation result for log (n) against redshift z for $\mathbf{z = 0}$ to $\mathbf{z = 5}$ of the standard Friedmann redshift model with $\boldsymbol{\lambda}$.

Preprints.org (www.preprints.org) | NOT PEER-REVIEWED | Posted: 10 September 2024 doi:10.20944/preprints202409.0780.v1

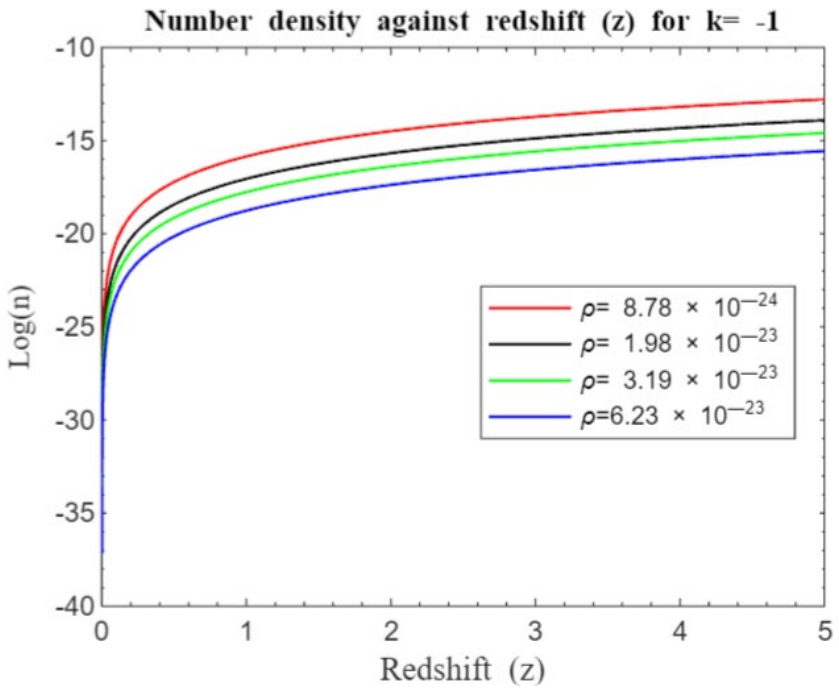

Figure 17. Simulation result for log (n) against redshift z for $\mathbf{z = 0}$ to $\mathbf{z = 5}$ of the standard Friedmann redshift model for an open universe without $\boldsymbol{\lambda}$.

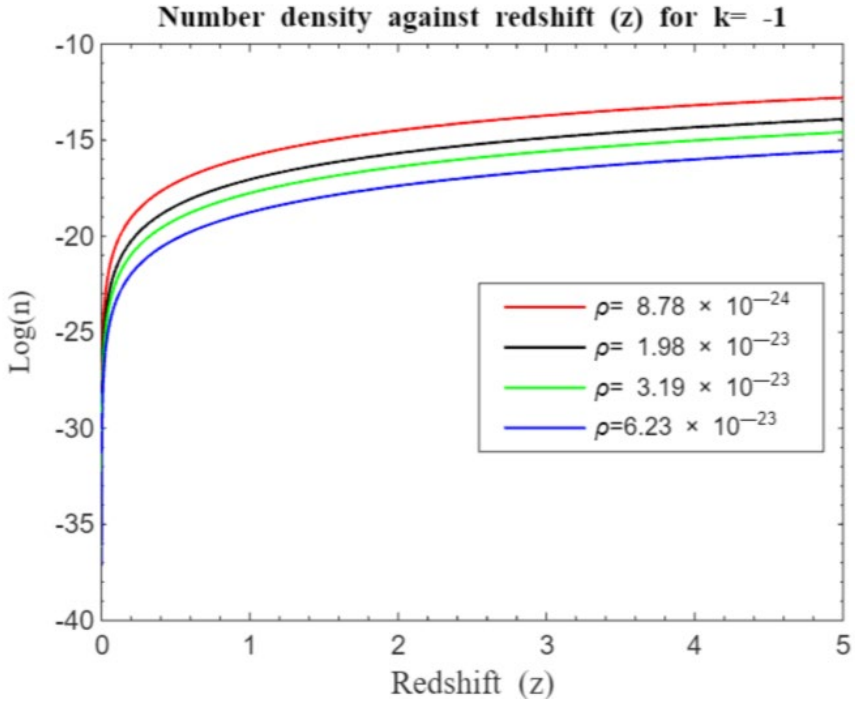

Figure 18. Simulation result for log (n) against redshift z for $\mathbf{z = 0}$ to $\mathbf{z = 5}$ of the standard Friedmann redshift model for an open universe with $\boldsymbol{\lambda}$.

Preprints.org (www.preprints.org) | NOT PEER-REVIEWED | Posted: 10 September 2024 doi:10.20944/preprints202409.0780.v1

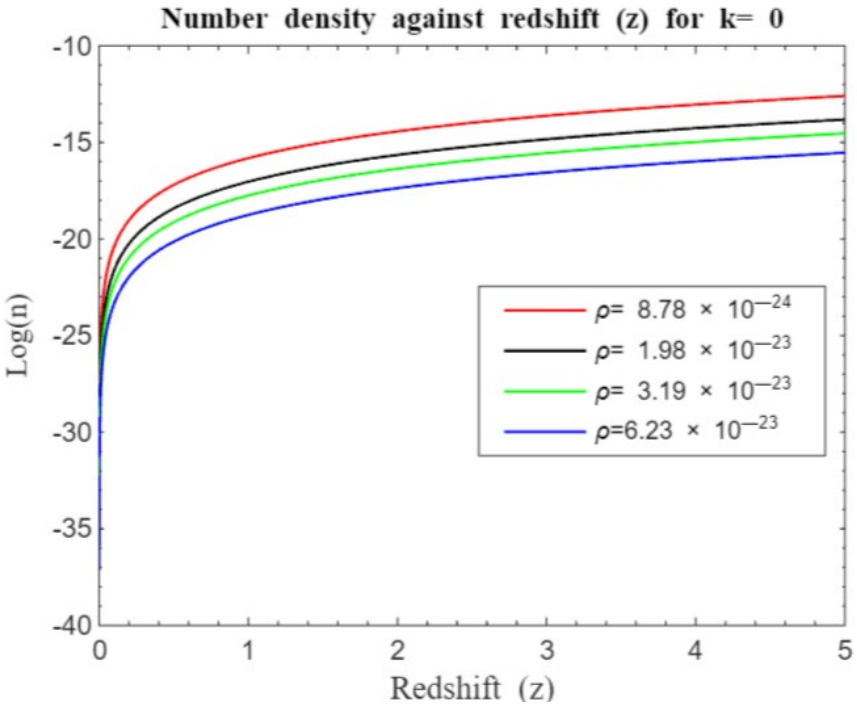

Figure 19. Simulation result for log (n) against redshift z for $\mathbf{z = 0}$ to $\mathbf{z = 5}$ of the standard Friedmann redshift model for a flat universe without $\boldsymbol{\lambda}$.

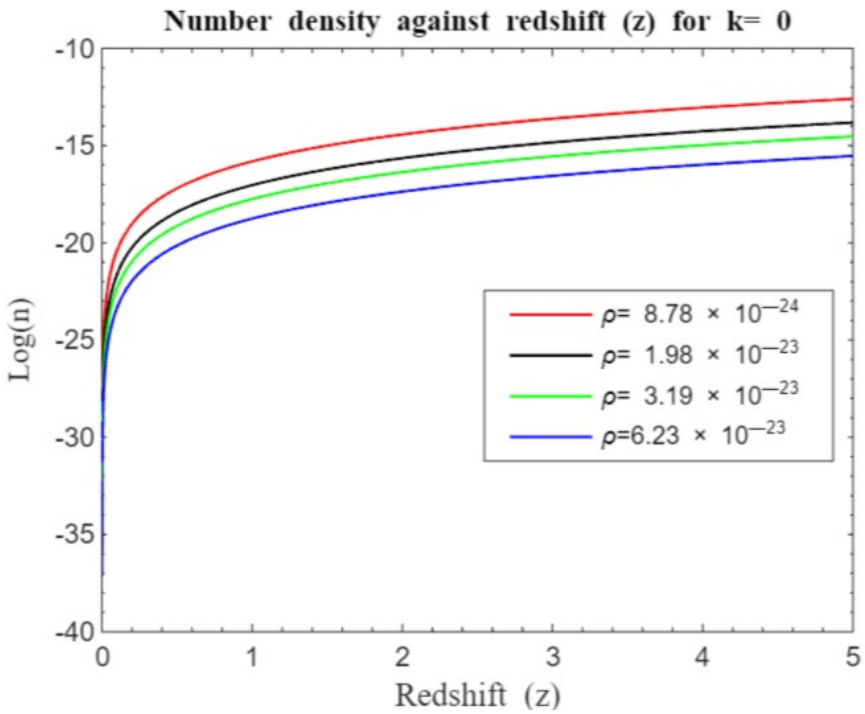

Figure 20. Simulation result for log (n) against redshift z for $\mathbf{z = 0}$ to $\mathbf{z = 5}$ of the standard Friedmann redshift model for a flat universe with $\boldsymbol{\lambda}$.

 doi:10.20944/preprints202409.0780.v1

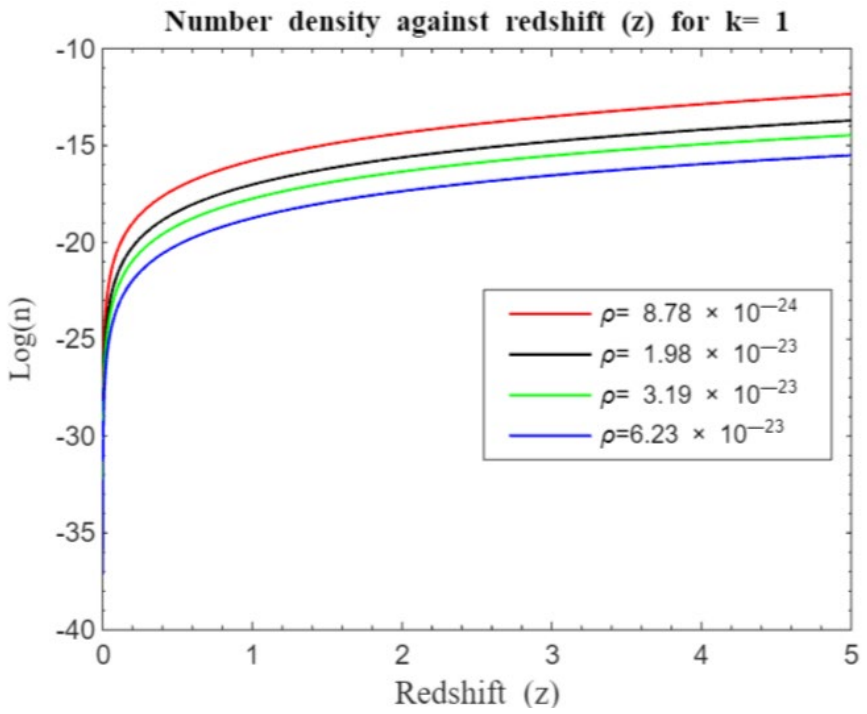

Figure 21. Simulation result for log (n) against redshift z for $\mathbf{z = 0}$ to $\mathbf{z = 5}$ of the standard Friedmann redshift model for a closed universe without $\boldsymbol{\lambda}$.

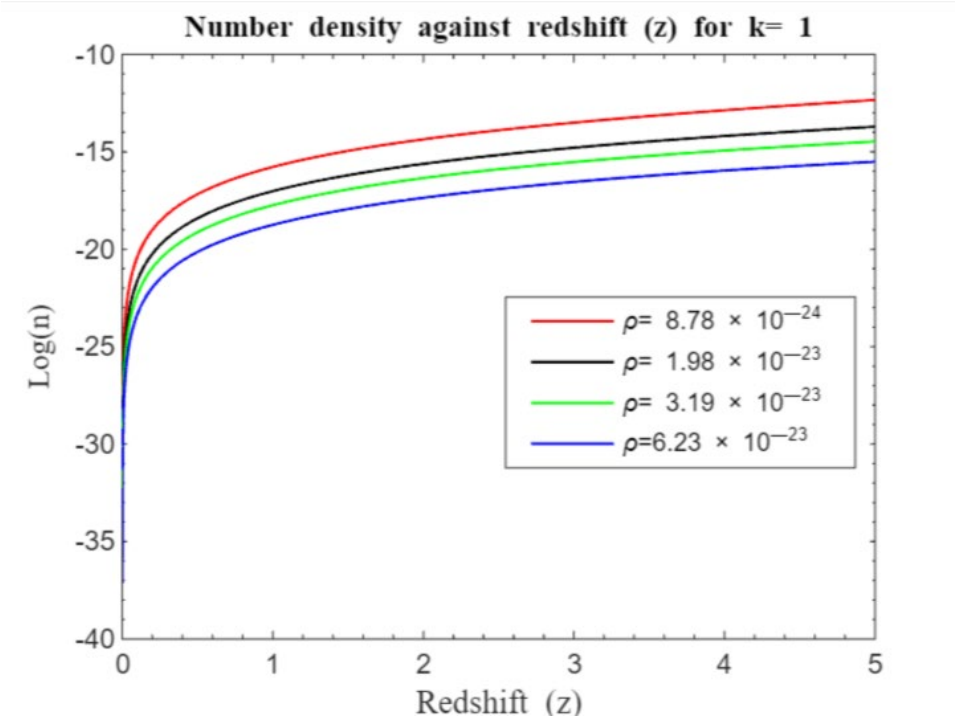

Figure 22. Simulation result for log (n) against redshift z for $\mathbf{z = 0}$ to $\mathbf{z = 5}$ of the standard Friedmann redshift model for a closed universe with $\boldsymbol{\lambda}$.

Preprints.org (www.preprints.org) | NOT PEER-REVIEWED | Posted: 10 September 2024 doi:10.20944/preprints202409.0780.v1

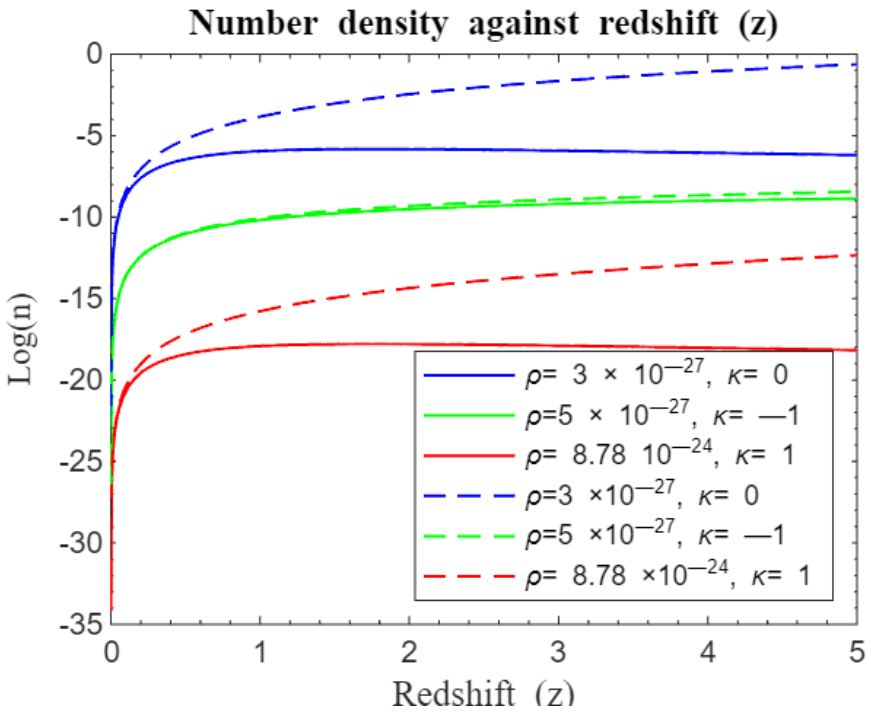

Figure 23. Simulation result for log (n) against redshift z for z = 0 to z = 5. The solid curves represent the approximate standard Friedmann redshift model while dotted curves represent the standard Friedmann redshift model. Both models without λ.

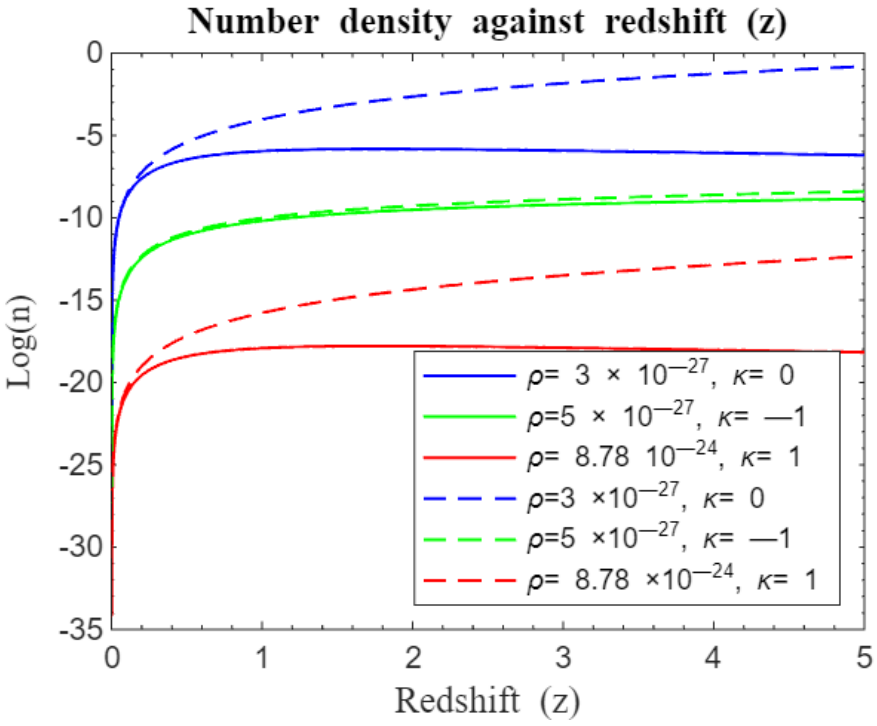

Figure 24. Simulation result for log (n) against redshift z for $\mathbf{z = 0}$ to $\mathbf{z = 5}$. The solid curves represent the approximate standard Friedmann redshift model without $\boldsymbol{\lambda}$ while dotted curves represent the standard Friedmann redshift model with λ.

Preprints.org (www.preprints.org) | NOT PEER-REVIEWED | Posted: 10 September 2024 doi:10.20944/preprints202409.0780.v1

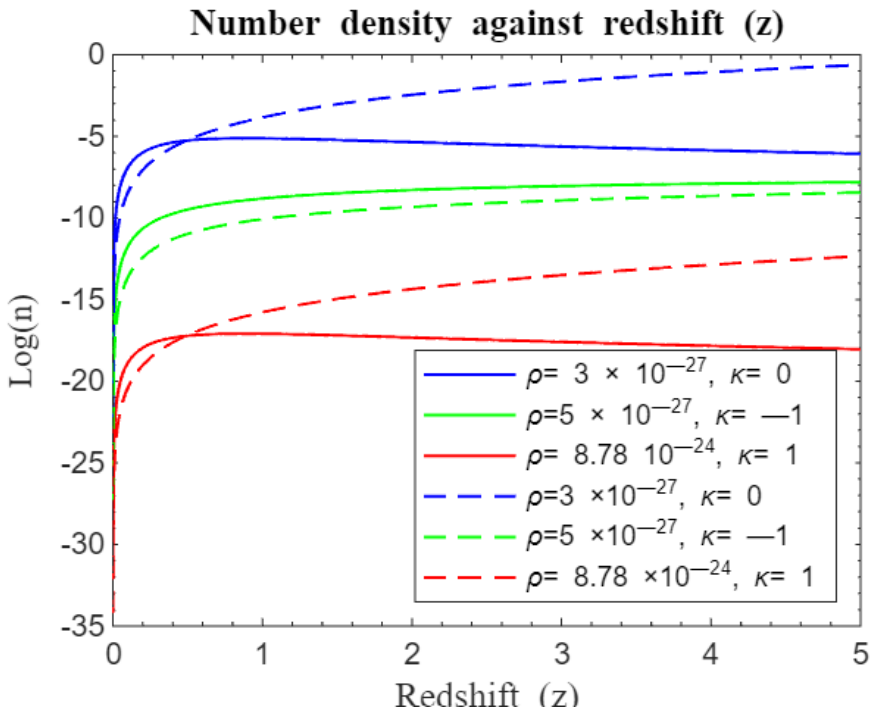

Figure 25. Simulation result for log (n) against redshift z for $\mathbf{z = 0}$ to $\mathbf{z = 5}$. The solid curves represent the modified standard Friedmann redshift $\mathbf{f(z) = \alpha_1 z + \alpha_2 z^2}$ with $\mathbf{\alpha_1 = 2.005}$ and $\mathbf{\alpha_2 = 0.005}$ of the approximate standard Friedmann model while dotted curves represent the standard Friedmann redshift model. Both models without λ.

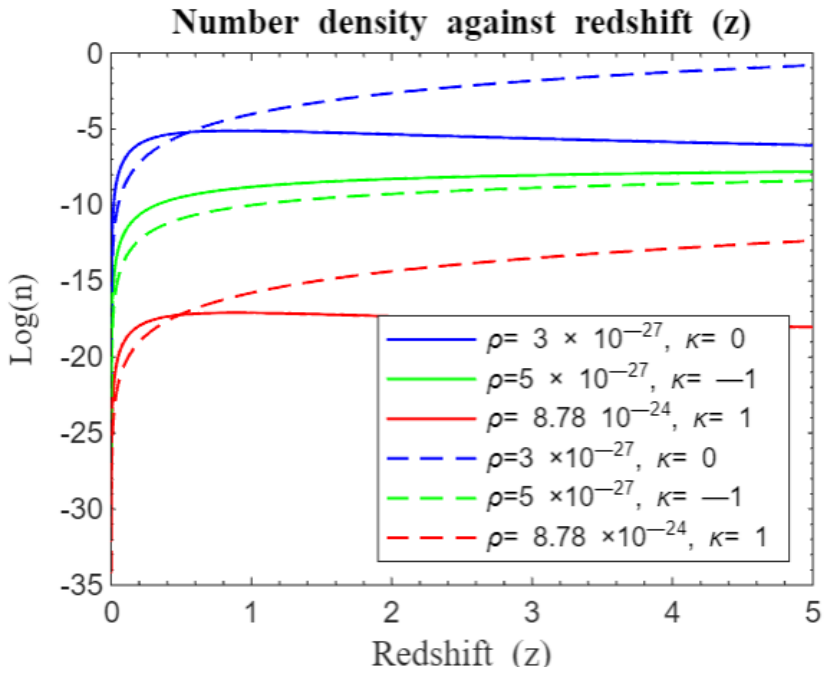

Figure 26. Simulation result for log (n) against redshift z for $\mathbf{z = 0}$ to $\mathbf{z = 5}$. The solid curves represent the modified standard Friedmann redshift $\mathbf{f(z) = \alpha_1 z + \alpha_2 z^2}$ with $\mathbf{\alpha_1 = 2.005}$ and $\mathbf{\alpha_2 = 0.005}$ of the approximate standard Friedmann redshift model without $\boldsymbol{\lambda}$ in a matter dominated universe while dotted curves represent the standard Friedmann redshift model with $\boldsymbol{\lambda}$.

Preprints.org (www.preprints.org) | NOT PEER-REVIEWED | Posted: 10 September 2024 doi:10.20944/preprints202409.0780.v1

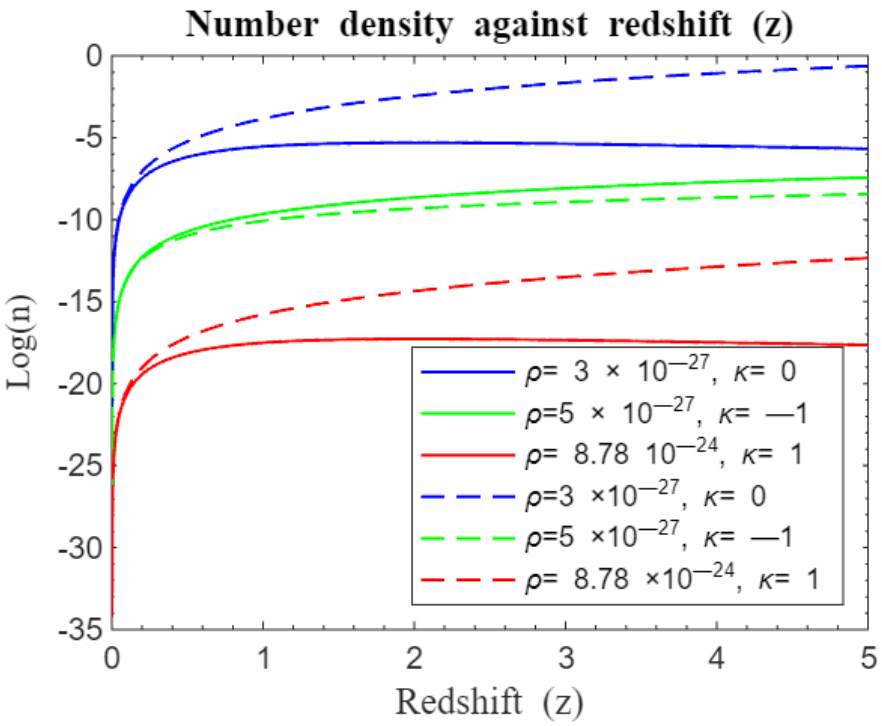

Figure 27. Simulation result for log (n) against redshift z for $\mathbf{z = 0}$ to $\mathbf{z = 5}$. The solid curves represent the modified standard Friedmann redshift $\boldsymbol{f(z) = z + \gamma(z)^2}$ with $\boldsymbol{\gamma = 0.45}$ of the approximate standard Friedmann redshift model while dotted curves represent the standard Friedmann redshift model. Both models without λ.

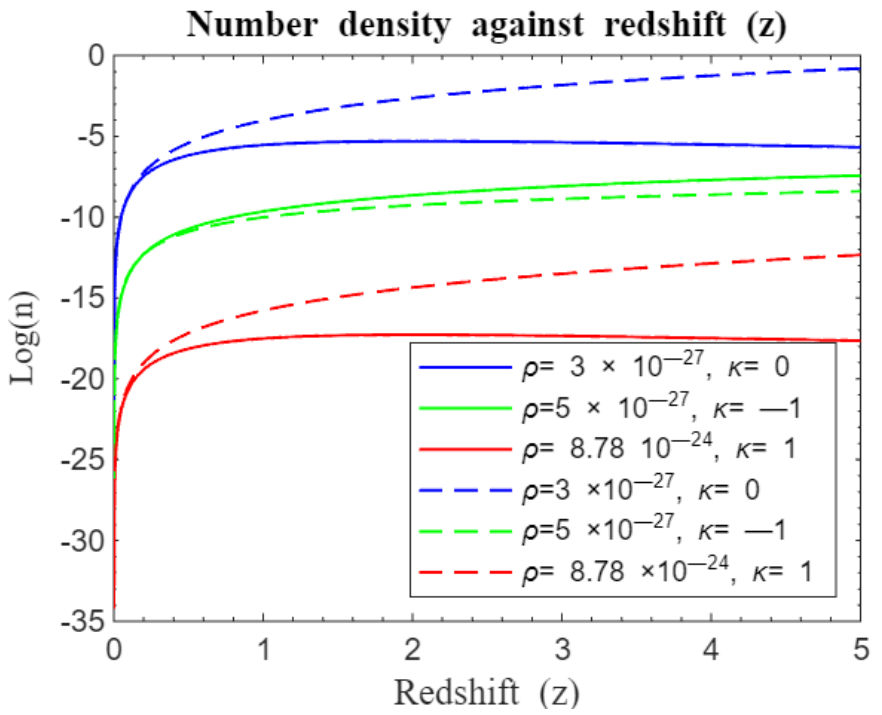

Figure 28. Simulation result for log (n) against redshift z for $\mathbf{z = 0}$ to $\mathbf{z = 5}$. The solid curves represent the modified standard Friedmann redshift $\mathbf{f(z) = z + \gamma(z)^2}$ with $\boldsymbol{\gamma = 0.45}$ of the approximate standard Friedmann redshift model without $\boldsymbol{\lambda}$ while dotted curves represent the standard Friedmann redshift model with $\boldsymbol{\lambda}$.

5. Discussion

 doi:10.20944/preprints202409.0780.v1

5.1. Light Intensity Redshift Relation

In cosmological studies, the relationship between light intensity and redshift is a crucial indicator of galaxy formation and the evolution of large-scale structures. Let us consider the relationship between light intensity and redshift in light of structure formation.

Figure 1-14 demonstrates an exponential decay in light intensity with increasing redshift, consistent with classical theory. This decay results from the dilution of photons as the universe expands. As the universe grows, the wavelengths of photons stretch, causing a decrease in their energy density. This effect arises because the number of photons remains constant while they are distributed over an increasingly larger volume [7,8,21,22].

Figures 1 and 2 compare light intensity-redshift relationships under different geometries, both without and with the cosmological constant. These Figures reveal that in a flat universe, light intensity decays more rapidly compared to an open or closed universe.

Figures 3-8 illustrate how light intensity changes with redshift across various densities and curvatures. A significant drop in intensity is observed at redshifts $0 < z < 0.5$, with a more gradual decline at higher redshifts. At lower redshifts, the universe is relatively young, which influences intensity. As redshift increases, light comes from increasingly distant regions. The slower intensity decay at higher redshifts may result from cumulative factors like distance, cosmic expansion, and the evolving structure of the universe, reflecting the intricate interplay of spatial distance, temporal evolution, and cosmic morphology (Riess et al., 1998).

In a universe with positive curvature, a closed model akin to a spherical structure is represented. Here, we still observe light attenuation with increase in redshift. A case of positive curvature points to a closed universe whose 3-D space is similar to the surface of a sphere in which the r-sphere wipes out the entire universe leaving it unbounded as the coordinates of the sphere varies from 1 to 0. We observe that light curves seem not to converge for positive curvature according to our model in contrast to earlier works [12,20]. As the redshift parameter (z) increases, these geometric differences become more pronounced, showing how curvature affects light behavior. In all geometries, light intensity curves decay more rapidly at lower densities compared to higher densities.

Figures 9-14 compare our model with those from previous studies [12,20]. These Figures show that high-density universes consistently exhibit higher initial light intensity at early times, regardless of the model. This implies that a denser universe leads to stronger early cosmic structures with higher light intensity. The gradual decline over time in such models suggest that denser universes, with stronger gravitational influences, retain light longer due to slower expansion rates. In contrast, a flat universe ($\kappa = 0$) shows moderate initial intensity and a steady decrease, while an open universe ($\kappa = -1$) exhibits a lower initial intensity and rapid decline, indicating that accelerated expansion reduces observable light intensity quickly. A closed universe ($\kappa = 1$) shows higher initial intensity and a more prolonged decline, reflecting a slower expansion rate.

Figures 9-10 compares our standard Friedmann redshift model with the approximate standard Friedmann redshift model proposed by Langa et al. (2017). Figure 10, which includes the cosmological constant, highlights the role of dark energy. Dark energy is known to accelerate the universe's expansion [13,14] . The approximate standard Friedmann redshift model suggests that early cosmic structures had higher initial light intensities with a slower decline, indicating that matter's gravitational influence moderate expansion and preserves light intensity. In contrast, the standard Friedmann redshift model shows lower initial light intensity and a more rapid decline, implying that insufficient matter to stabilize the expansion leads to faster reduction in light from early structures.

Further comparison with Nyagisera et al. (2024), who modified the approximate standard Friedmann redshift model with non-parametric (Figures 11-12) and parametric (Figures 13-14) redshift functions, provides additional insights. Figures 11-12 show that light attenuation is more pronounced in the standard Friedmann redshift model compared to the modified standard Friedmann redshift nonparametric model. Even without dark energy, as indicated by the absence of a cosmological constant, the universe still experiences accelerated expansion, suggesting a significant role of dark matter in driving expansion and redshifting of light [12].

 doi:10.20944/preprints202409.0780.v1

Figures 13-14 exhibit similar trends in light attenuation with increasing redshift, particularly between redshifts 0 and 1, where attenuation is rapid for flat and closed geometries except in open geometry where our model attenuates slower than parametric model. The standard Friedmann redshift model shows faster attenuation compared to the modified standard Friedmann redshift parametric model, potentially due to factors like photon-electron recombination, Thomson scattering, or accelerated expansion. The absence of a cosmological constant in Figure 13 implies that dark matter may primarily be responsible for driving accelerated expansion, overshadowing the cosmological constant's effects.

5.2. Number Density Redshift Relation

The number density redshift relation helps astronomers understand how the number of galaxies changes over time. By studying how galaxy number density evolves with redshift, scientists can infer the processes of galaxy formation, growth, and the effects of cosmic expansion on galactic structures. We shall, in particular, focus on the processes of galaxy formation and evolution. Our overall simulations (see Figures 15-28) show that the number density of galaxies generally rises at the beginning from $z = 0$ and grows at uneven rate until a plateau before declining, leveling or showing slight rate of increase regardless of the model used. In particular, our model in Figures 15-22 show that there is rapid structure formation at the beginning of the universe for $0 < z < 0.5$ which gradually rises up to around $z \approx 0.8$ before structure formation proceeds at a slower rate regardless of the curvature and density of the universe. However, our standard Friedmann redshift model shows that the presence of a cosmological constant seems not to have pronounced impact on structure formation showing that dark energy presence seem to have negligible effects on galaxy formation in contrast to earlier works [20]. This may probably be because dark energy primarily affects the large-scale expansion of the universe rather than local gravitationally bound systems like galaxies or galaxy clusters. It is believed that on small scales, gravity, driven by dark matter and ordinary matter, dominates over the effects of dark energy. However, the effect of dark matter seems to go beyond small-scale influence and dominates over dark energy for all redshift ranges as far as our model investigation is concerned.

We compared our simulations on structure formation with earlier works of Langa et al. (2017) as depicted by Figures 23-24. It is clear from these simulations that structure formation for both approximate standard Friedmann redshift model and standard Friedmann redshift model experienced similar rapid galaxy formation rate for both closed and flat universes at early times until $z \approx 0.1$ before our model (standard Friedmann redshift model) made a sharp departure from approximate standard Friedmann model [20]. It is also noted that for both models, the open universe curves do not deviate from each other at early times and tend to follow similar structure formation trajectories with our model slightly having an edge over its counterpart in terms of galaxy formation rate at late times. After the point of departure, structure formation for both closed and flat universes in our model continued steadily but at reduced rate unlike its counterpart that reached a plateau around $z \approx 0.5$ then after this, they started to decline while open universe leveled off in growth. It is also clear that the effect of a cosmological constant associated with dark energy is less impactful as demonstrated by results of Figures 23-24. This shows that structural growth of galaxies is influenced by dark Matter much more than dark energy. This emphasizes the fact that dark matter is associated with accelerated expansion of the universe and arises as an emergent phenomenon as posited by phenomenological models [10–12,23] .

We again proceeded to compare our model with Nyagisera et al. (2024) as depicted by simulation results in Figures 25-28. Our model was compared with the modified standard Friedmann redshift model for parametric and nonparametric functions as shown in Figures 25-26 and 27-28 respectively. It is evident from Figures 25-26 that there was rapid structure formation at the beginning of the universe for the modified standard Friedmann redshift parametric models than our standard Friedmann redshift model until redshift $z \approx 0.5$ when formation rate was now same and divergent of curves followed hereafter. Structure formation consequently changed with our model maintaining a stead but less rapid galaxy formation for both closed and flat universe after $z \approx 0.5$. However, there

 doi:10.20944/preprints202409.0780.v1

is obvious departure for curves of open universe right from the onset of structure formation with our model trailing in number density at early epoch but trying to catch up at later times. On the other hand, modified standard Friedmann redshift nonparametric model in Figures 27-28 compares with our standard Friedmann redshift model in such a way that structure formation rate is similar at the beginning of the universe for both closed and flat universe only diverging after $z \approx 0.2$. Hereafter, curves from our model depict steady galaxy formation for both closed and flat universe. However, the green curves depicting an open universe follow a similar trajectory to the modified parametric curves, starting together and only differing infinitesimally at later times with ours slightly below the modified parametric green curve. The two universes reach a plateau at $z \approx 0.5$ before structure formation proceeds at a constant rate. From Figures 15-28, we observe high activity in galaxy formation rate at the beginning of the universe than at later times. Formation of cosmic structures seem to have been faster at redshifts up to $0 < z < 0.5$ after which it slowed down. Galaxy formation is influenced by a variety of factors including the density fluctuations in the early universe and the nature of dark matter. In the early universe, density fluctuations provided the seeds for the formation of structures like galaxies. These fluctuations were more pronounced at smaller redshifts, corresponding to earlier times in the universe's history. As the universe expanded, the density of matter decreased, leading to slower galaxy formation over time [24]. Dark matter, which constitutes a significant portion of the universe's mass, plays a crucial role in galaxy formation by gravitationally attracting ordinary matter. Studies have shown that dark matter halos, which host galaxies, grow more rapidly at smaller redshifts due to the higher density of matter in the early universe [13,25]. This observation is in agreement with our results. Also, feedback processes, including supernova explosions and black hole activity, regulate the rate of star formation within galaxies. As the universe ages and galaxies evolve, these feedback mechanisms become more efficient, leading to a slowdown in the formation of new stars or galaxies. This observation well aligns with our findings where we observed that galaxy formation slowed time at later times when $z > 0.8$. Observations and simulations, like those conducted by Péroux et al. [26], highlight the importance of feedback in shaping galaxy properties over cosmic time. Recent observational studies, such as those analyzed by Huterer & Shafer [27], indicate that as the universe expands, the gravitational pull between galaxies weakens, contributing to a slowdown in the formation of new galaxies at higher redshifts in tandem with our findings. These factors collectively contribute to the observed trend of faster galaxy formation at smaller redshifts and a gradual decrease in the rate of formation as redshifts increase or as the universe expands. This balanced expansion results in a relatively stable number density of objects over cosmic time [28]. In an open universe with negative curvature, the spatial geometry is hyperbolic, and the expansion continues indefinitely without a collapse. Similarly, in the flat universe, the expansion may decelerate due to matter density, but the presence of dark matter again may lead to an accelerated expansion. This continuous expansion results in a gradual decrease in the growth rate of large-scale structure, leading to a flattening of the number density vs redshift curve [6,29]. In a universe with positive curvature, the spatial geometry resembles that of a hypersphere. As the universe evolves, the gravitational attraction due to the matter density eventually overcomes the expansion driven by dark energy, leading to a collapse of the universe. This collapse results in a rapid decrease in the observed number density of objects (such as galaxies) as redshift increases [30]. In our case, we did not observe substantial impact of dark energy so that its effect may have been overshadowed by dark matter effects.

5.3. Comparison with Observational Data

The study of redshift in galaxies stands as a cornerstone in our quest to understand the processes of structure formation, and evolutionary in the universe.

Central to our task, we embarked on the utilization of vast and accurate astronomical datasets of our present time, teeming with measurements of redshift and number density. These datasets are curated to ensure accuracy and freedom from the effects of background geometry or cosmic distance measurement anomalies as much as possible. Leveraging on these datasets, we embarked on comparative analysis, extracting plots that mirrored the parameters of our analytical models. This

 doi:10.20944/preprints202409.0780.v1

alignment in scale facilitates a direct comparison between the theoretical constructs delineated by our model and the empirical realities captured by observational data.

We collected observed redshifts between 0 and 5, specifically, for extragalactic galaxies in the infrared spectral region, using Planck 2015 cosmological parameters from the NASA/IPAC Extragalactic Database (NED) (https://ned.ipac.caltech.edu/; [31]. The distribution of these retrieved redshifts was plotted, with the bin heights indicating the number of galaxies observed at each redshift, as shown in Figure 29.

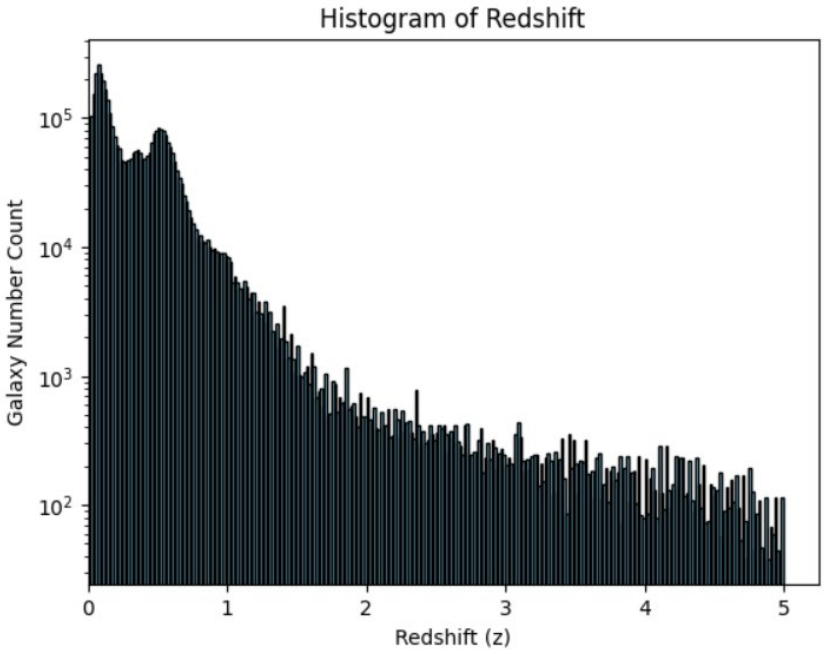

Figure 29. Redshift distribution for NED observed galaxies in infrared spectral region. Source: https://ned.ipac.caltech.edu/.

In Figure 29, an exponential decrease in the distribution of observed galaxies with increase in redshift was observed. Clearly, there was high activity of galaxy formation in the redshift range $0 < z < 1.5$ with a burst of galaxies forming between $0 < z < 0.8$ and presenting two characteristic peaks at $z \approx 0.1$ and $z \approx 0.5$. This indicated that galaxies were formed at a faster rate in the beginning of the universe $z < 1$ than at later time. It is interesting to note that this observational data exactly coincides with our theoretical model predictions of galaxy formation peaks at $z \approx 0.5$ and $z \approx 0.1$ as presented by Figures 15-22 and Figures 23-24 respectively. This alignment therefore, validates our Friedmann model adopted in this work as a correct cosmological framework for accounting of structure formation and evolution in the universe.

6. Summary and Conclusions

The cosmological principle, a fundamental assumption in the standard cosmological model, posits that the universe is homogeneous and isotropic at large scales, though this is not evident on smaller scales. The Friedmann-Lemaitre-Robertson-Walker metric serves as the foundation of modern cosmology, with deviations from the standard model addressing challenges such as the Hubble tension and cosmic coincidence problems. Redshift-distance and light intensity-distance relations are critical tools for testing the validity of cosmological models, especially with the rise of both parametric and nonparametric redshift models.

Dark matter and dark energy play significant roles in explaining galaxy formation and cosmic expansion, though their nature remains largely unknown. Observational methods, such as three-dimensional redshift surveys, present challenges in affirming large-scale homogeneity. Discrepancies

 doi:10.20944/preprints202409.0780.v1

between observations, such as quasar distribution studies, and the expected homogeneity, indicate that further analysis is needed.

This study aims to refine our understanding of the universe's structure by focusing on three key astronomical parameters: number density, light intensity, and redshift. It examines the evolution of these quantities from the early universe to the present and compares findings with both the 'approximate standard Friedmann redshift model' by Langa et al. (2017) and the 'modified standard Friedmann redshift model' by Nyagisera et al. (2024). The study introduces the 'standard Friedmann redshift model,' which incorporates the effects of dark matter and dark energy.

The study establishes that light intensity decays exponentially with increasing redshift due to the universe's expansion. This relationship, confirmed by Figures 1-14, is in agreement with our classical expectation that attribute the decrease in energy density to photon dilution as the universe expands.

The results highlight that the geometry of the universe significantly impacts light intensity. In a flat universe, light intensity decays more rapidly compared to an open or closed universe, as shown in Figures 1 and 2. For example, a closed universe ($\kappa = 1$) displays higher initial intensity with a slower decline, while an open universe ($\kappa = -1$) shows a faster drop in light intensity. Comparative analysis of models reveals that high-density universes exhibit higher initial light intensities during early times.

Figures 15-22 indicate that dark energy has negligible effects on structure formation, contrasting with earlier works of Langa et al (2017) and Nyagisera et al (2024). This emphasizes the fact that dark matter, rather than dark energy, drives galaxy formation by influencing local gravitationally bound systems and even beyond.

Furthermore, the study shows that galaxy formation occurred more rapidly at early times, particularly within the redshift range $0 < z < 0.5$, as illustrated by Figures 15-28. This aligns with the idea that density fluctuations in the early universe, amplified by dark matter, were key in facilitating early galaxy formation.

Observational data from the NASA/IPAC Extragalactic Database, presented in Figure 29, reinforces these findings by showing that there was a galaxy burst between redshifts 0 and 1, which peaked around $z \approx 0.1$ and $z \approx 0.5$. These characteristic redshift peak values are consistent with our theoretical predictions of the standard Friedmann redshift model used in this work (see Figures 15-22 and Figures 23-24 respectively), validating its accuracy in explaining the formation and evolution of cosmic structures.

In conclusion, this work therefore, presents a formidable understanding of the relationship between light intensity, redshift, and structure formation in the universe, while emphasizing the pivotal role of dark matter and cosmic geometry in shaping the universe's evolution.

The implications of this work extend into several key areas for future research. First, a more subtle approach is needed to model the structure and evolution of the universe, one that better accounts for the complexities of dark energy's and dark matter's influence on galaxy formation. Second, our results call for more detailed observational campaigns targeting the redshift ranges identified in this study to further investigate the underlying mechanisms driving these processes.

Furthermore, the growing challenges to the cosmological principle suggest that alternative models of the universe, potentially those that allow for more variation on large scales, should be considered.

Lastly, the evidence of rapid galaxy formation at specific redshifts and the crucial role of dark matter in shaping cosmic structures point to gaps in our current understanding that require further exploration.

Author Contributions: Conceptualization, Dismas Wamalwa; Data curation, Patrick Mwaniki; Formal analysis, Dickson Kinyua; Methodology, Dismas Wamalwa; Software, Daniel Maitethia; Supervision, Dismas Wamalwa, Dickson Kinyua and Daniel Maitethia; Visualization, Dismas Wamalwa; Writing – original draft, Kennedy Konga.

Funding: This research received no external funding.

Institutional Review Board Statement: Not applicable.

Informed Consent Statement: Not applicable.

Data Availability: Data underlying this article can be provided from the corresponding author upon request. Also, it can be retrieved from NED database (https://ned.ipac.caltech.edu/) using the search by parameters described in this article.

Acknowledgement: This research has made use of the NASA/IPAC Extragalactic Database (NED), which is operated by the Jet Propulsion Laboratory, California Institute of Technology, under contract with the National Aeronautics and Space Administration.

Conflicts of Interest: The authors declare no conflict of interest.

References

1. Einstein, A.: On the special and general theory of relativity. CPAE Engl. Transl. 6, 247–420 (1917).
2. Park, C.-G., Hyun, H., Noh, H., Hwang, J.: The cosmological principle is not in the sky. Mon. Not. R. Astron. Soc. 469, 1924–1931 (2017).
3. Melia, F.: The Friedmann–Lemaître–Robertson–Walker metric. Mod. Phys. Lett. A. 37, 2250016 (2022). https://doi.org/10.1142/S021773232250016X.
4. Melia, F.: A candid assessment of standard cosmology. Publ. Astron. Soc. Pac. 134, 121001 (2022).
5. Wang, M., Fu, X., Xu, B., Yang, Y., Chen, Z.: Testing the FLRW metric with the Hubble and transversal BAO measurements, http://arxiv.org/abs/2305.01268, (2023).
6. Aluri, P.K., Cea, P., Chingangbam, P., Chu, M.-C., Clowes, R.G., Hutsemékers, D., Kochappan, J.P., Lopez, A.M., Liu, L., Martens, N.C.: Is the observable Universe consistent with the cosmological principle? Class. Quantum Gravity. 40, 094001 (2023).
7. Díaz-Pachón, D.A., Hössjer, O., Marks, R.J.: Sometimes size does not matter. Found. Phys. 53, 1 (2023).
8. Krishnan, C., Mohayaee, R., Colgáin, E.Ó., Sheikh-Jabbari, M.M., Yin, L.: Does Hubble tension signal a breakdown in FLRW cosmology? Class. Quantum Gravity. 38, 184001 (2021).
9. Weinberg, S.: The cosmological constant problem. Rev. Mod. Phys. 61, 1–23 (1989). https://doi.org/10.1103/RevModPhys.61.1.
10. Bassett, B.A., Fantaye, Y., Hlozek, R., Sabiu, C., Smith, M.: A tale of two redshifts. ArXiv Prepr. ArXiv13122593. (2015).
11. Wojtak, R., Prada, F.: Redshift remapping and cosmic acceleration in dark-matter-dominated cosmological models. Mon. Not. R. Astron. Soc. 470, 4493–4511 (2017).
12. Nyagisera, R.N., Wamalwa, D., Rapando, B., Awino, C., Mageto, M.: A Critical Examination of the Standard Cosmological Model: Toward a Modified Framework for Explaining Cosmic Structure Formation and Evolution. Astronomy. 3, 43–67 (2024).
13. Jeakel, A.P., da Silva, J.P., Velten, H.: Revisiting f (R, T) cosmologies. Phys. Dark Universe. 43, 101401 (2024).
14. Farnes, J.S.: A unifying theory of dark energy and dark matter: Negative masses and matter creation within a modified ΛCDM framework. Astron. Astrophys. 620, A92 (2018).
15. Blake, C., Wall, J.: Measurement of the angular correlation function of radio galaxies from the NRAO VLA Sky Survey. Mon. Not. R. Astron. Soc. 329, L37–L41 (2002).
16. Penzias, A.A., Wilson, R.W.: A measurement of the background temperature at 1415 MHz. Astron. J. Vol 72 P 315. 72, 315 (1967).
17. Pandey, B., Sarkar, S.: An information theory based search for homogeneity on the largest accessible scale. (2016).
18. Bernardo, R.C., Grandón, D., Said, J.L., Cárdenas, V.H.: Parametric and nonparametric methods hint dark energy evolution. Phys. Dark Universe. 36, 101017 (2022).
19. Wamalwa, D.S.: On the FriedmannCosmology. Int. J. Pure Apllied Math. 107, (2016). https://doi.org/10.12732/ijpam.v107i4.2.
20. Langa, M., Wamalwa, D.S., Mito, C.: Relativistic Dynamics in a Matter-Dominated Friedmann Universe. J. Astrophys. Astron. 38, 71 (2017). https://doi.org/10.1007/s12036-017-9482-5.
21. Ryden, B.: Introduction to Cosmology Addison Wesley. San Franc. USA. (2003).
22. Weinberg, S.: Cosmology. OUP Oxford (2008).
23. Wojtak, R., Prada, F.: Testing the mapping between redshift and cosmic scale factor. Mon. Not. R. Astron. Soc. 458, 3331–3340 (2016).
24. Aghanim, N., Akrami, Y., Ashdown, M., Aumont, J., Baccigalupi, C., Ballardini, M., Banday, A.J., Barreiro, R.B., Bartolo, N., Basak, S.: Planck 2018 results-VI. Cosmological parameters. Astron. Astrophys. 641, A6 (2020).
25. Wechsler, R.H., Zentner, A.R., Bullock, J.S., Kravtsov, A.V., Allgood, B.: The dependence of halo clustering on halo formation history, concentration, and occupation. Astrophys. J. 652, 71 (2006).

 doi:10.20944/preprints202409.0780.v1

26. Péroux, C., Nelson, D., van de Voort, F., Pillepich, A., Marinacci, F., Vogelsberger, M., Hernquist, L.: Predictions for the angular dependence of gas mass flow rate and metallicity in the circumgalactic medium. Mon. Not. R. Astron. Soc. 499, 2462–2473 (2020).
27. Huterer, D., Shafer, D.L.: Dark energy two decades after: observables, probes, consistency tests. Rep. Prog. Phys. 81, 016901 (2017).
28. Weinberg, D.H., Dave, R., Katz, N., Hernquist, L.: Galaxy clustering and galaxy bias in a ΛCDM universe. Astrophys. J. 601, 1 (2004).
29. Bond, J.R.: Large Scale Structure in Universes Dominated by Cold Dark Matter. In: Madore, B.F. and Tully, R.B. (eds.) Galaxy Distances and Deviations from Universal Expansion. pp. 255–263. Springer Netherlands, Dordrecht (1986).
30. Peebles, P.J.E.: The large-scale structure of the universe. Princeton university press (2020).
31. Ade, P.A., Aghanim, N., Arnaud, M., Ashdown, M., Aumont, J., Baccigalupi, C., Banday, A.J., Barreiro, R.B., Bartlett, J.G., Bartolo, N.: Planck 2015 results-xiii. cosmological parameters. Astron. Astrophys. 594, A13 (2016).